



THE UNIVERSITY *of* EDINBURGH

Edinburgh Research Explorer

## **Stomatal optimisation based on xylem hydraulics (SOX) improves land surface model simulation of vegetation responses to climate**

**Citation for published version:**

Eller, CB, Rowland, L, Mencuccini, M, Rosas, T, Williams, K, Harper, A, Medlyn, BE, Wagner, Y, Klein, T, Teodoro, GS, Oliveira, RS, Matos, IS, Rosado, BH, Fuchs, K, Wohlfahrt, G, Montagnani, L, Meir, P, Sitch, S & Cox, PM 2020, 'Stomatal optimisation based on xylem hydraulics (SOX) improves land surface model simulation of vegetation responses to climate', *New Phytologist*. <https://doi.org/10.1111/nph.16419>

**Digital Object Identifier (DOI):**

[10.1111/nph.16419](https://doi.org/10.1111/nph.16419)

**Link:**

[Link to publication record in Edinburgh Research Explorer](#)

**Document Version:**

Peer reviewed version

**Published In:**

New Phytologist

**Publisher Rights Statement:**

© 2020 The Authors New Phytologist © 2020 New Phytologist Trust

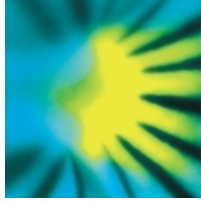
**General rights**

Copyright for the publications made accessible via the Edinburgh Research Explorer is retained by the author(s) and / or other copyright owners and it is a condition of accessing these publications that users recognise and abide by the legal requirements associated with these rights.

**Take down policy**

The University of Edinburgh has made every reasonable effort to ensure that Edinburgh Research Explorer content complies with UK legislation. If you believe that the public display of this file breaches copyright please contact [openaccess@ed.ac.uk](mailto:openaccess@ed.ac.uk) providing details, and we will remove access to the work immediately and investigate your claim.





# New Phytologist

## **Stomatal optimisation based on xylem hydraulics (SOX) improves land surface model simulation of vegetation responses to climate**

Journal:	<i>New Phytologist</i>
Manuscript ID	NPH-MS-2019-31667.R1
Manuscript Type:	MS - Regular Manuscript
Date Submitted by the Author:	n/a
Complete List of Authors:	Eller, Cleiton; University of Exeter, Department of geography Rowland, Lucy; University of Exeter, Department of Geography; University of Exeter, Department of Geography Mencuccini, Maurizio; CREAM, Universidad Autonoma de Barcelona, c/o, CREAM; Pg. Lluís Companys 23, ICREA Rosas, Teresa; Universitat Autonoma de Barcelona Centre de Recerca Ecologica i Aplicacions Forestals, Biologia Animal, Vegetal i Ecologia Medlyn, Belinda; Western Sydney University Hawkesbury Institute for the Environment, Ecosystem Function and Integration Williams, Karina; Met Office, Hadley Centre Harper, Anna; University of Exeter, College of Engineering, Mathematics and Physical Sciences Wagner, Yael; Weizmann Institute of Science, Department of Plant and Environmental Sciences Klein, Tamir; Weizmann Institute of Science, Department of Plant and Environmental Sciences Teodoro, Grazielle; University of Campinas, Plant Biology Oliveira, Rafael; University of Campinas, Plant Biology Matos, Iláine ; Universidade do Estado do Rio de Janeiro, Instituto de Biologia Roberto Alcântara Gomes Rosado, Bruno; Universidade do Estado do Rio de Janeiro, Ecologia; Fuchs, Kathrin; ETH Zurich Department of Environmental Systems Science, Department of Environmental Systems Science Wohlfahrt, Georg; University of Innsbruck, Ecosystem Research & Landscape Ecology Montagnani, Leonardo; Free University of Bolzano Faculty of Science and Technology, Faculty of Science and Technology Meir, Patrick; Australian National University, Research School of Biology; University of Edinburgh, School of Geosciences Sitch, Stephen; University of Exeter, College of Life and Environmental Sciences ; University of Leeds, School of Geography Cox, Peter; University of Exeter, School of Engineering, Mathematics and Physical Sciences
Key Words:	climate change, drought, eddy covariance, land-surface models, stomata optimization models, xylem hydraulics



SCHOLARONE™  
Manuscripts

1 **Stomatal optimisation based on xylem hydraulics (SOX) improves land surface model**  
 2 **simulation of vegetation responses to climate**

3 Eller CB<sup>1,2</sup>, Rowland L<sup>1</sup>, Mencuccini M<sup>3,4</sup>, Rosas T<sup>3,4</sup>, Williams K<sup>5</sup>, Harper A<sup>6</sup>, Medlyn BE<sup>7</sup>,  
 4 Wagner Y<sup>8</sup>, Klein T<sup>8</sup>, Teodoro GS<sup>9</sup>, Oliveira RS<sup>2</sup>, Matos IS<sup>10</sup>, Rosado BHP<sup>10</sup>, Fuchs K<sup>11</sup>,  
 5 Wohlfahrt G<sup>12</sup>, Montagnani L<sup>13</sup>, Meir P<sup>14,15</sup>, Sitch S<sup>1</sup>, Cox PM<sup>6</sup>

6 <sup>1</sup>College of Life and Environmental Sciences, University of Exeter, Exeter, EX4 4QF, UK; <sup>2</sup>Department of  
 7 Plant Biology, University of Campinas, Campinas, 13083-862, Brazil; <sup>3</sup>CREAF, Barcelona, Spain.

8 <sup>4</sup>ICREA, Barcelona, Spain; <sup>5</sup>Met Office Hadley Centre, Fitzroy Road, Exeter, EX1 3PB, UK; <sup>6</sup>College of  
 9 Engineering, Mathematics and Physical Sciences, University of Exeter, Exeter, EX4 4QF, UK;

10 <sup>7</sup>Hawkesbury Institute for the Environment, Western Sydney University, Locked Bag 1797, Penrith NSW  
 11 2751 Australia; <sup>8</sup>Department of Plant & Environmental Sciences, Weizmann Institute of Science, 76100

12 Rehovot, Israel; <sup>9</sup>Institute of Biological Sciences, Federal University of Pará, Belém, 66075-110, Brazil;

13 <sup>10</sup>Department of Ecology - IBRAG, Rio de Janeiro State University (UERJ), 20550-013, Brazil;

14 <sup>11</sup>Department of Environmental Systems Science, ETH Zurich, Universitätstrasse 2,8092 Zurich,  
 15 Switzerland; <sup>12</sup>Department of Ecology, University of Innsbruck, Innsbruck, 6020, Austria; <sup>13</sup>Forest

16 Services, Autonomous Province of Bolzano, Via Brennero 6, 39100 Bolzano, Italy; <sup>14</sup>Research School of  
 17 Biology, The Australian National University, Acton ACT 2601, Australia; <sup>15</sup>School of Geosciences,  
 18 University of Edinburgh, Edinburgh EH93FF, UK

19

20 Author for correspondence:

21 *Cleiton B. Eller*

22 *Email: c.breder-eller@exeter.ac.uk*

23

Main text word count	6420	No. figures	6 (all color)
Summary	190	No. of Supporting Information files	1
Introduction	1174		
Material and Methods	1948		
Results	1441		
Discussion	1857		
Acknowledgments	118		
No. Tables	3		

24

## 25 **Summary**

- 26 • Land surface models (LSMs) typically use empirical functions to represent vegetation  
27 responses to soil drought. These functions largely neglect recent advances in plant  
28 ecophysiology that link xylem hydraulic functioning with stomatal responses to climate.
- 29 • We developed an analytical stomatal optimisation model based on xylem hydraulics (SOX)  
30 to predict plant responses to drought. Coupling SOX to the Joint UK Land Environment  
31 Simulator (JULES) LSM, we conducted a global evaluation of SOX against observations.
- 32 • SOX simulates leaf stomatal conductance responses to climate for woody plants more  
33 accurately and parsimoniously than the existing JULES stomatal conductance model. An  
34 ecosystem-level evaluation at 70 eddy flux sites shows that SOX decreases the sensitivity  
35 of gross primary productivity (GPP) to soil moisture, which improves the model agreement  
36 with observations and increases the predicted annual GPP by 30%. SOX decreases JULES  
37 root mean squared error in GPP by up to 45 % in evergreen tropical forests, and can  
38 simulate realistic patterns of canopy water potential and soil water dynamics at the studied  
39 sites.
- 40 • SOX provides a parsimonious way to incorporate recent advances in plant hydraulics and  
41 optimality theory into LSMs, and an alternative to empirical stress factors.

42 **Keywords:** climate change, drought, eddy covariance, land-surface models, stomatal  
43 optimization, xylem hydraulics.

44

45

46

47

## 48 Introduction

49 Large areas of the globe will be exposed to increased aridity in the near future (Sheffield &  
50 Wood, 2008; Duffy *et al.*, 2015; Marengo *et al.*, 2018). As drought events become more intense  
51 and frequent, accurately representing vegetation-climate feedbacks in Earth System Models  
52 (ESMs) is increasingly important, as these interactions can drastically influence model projections  
53 of global climate change (Cox *et al.*, 2000). The current generation of Land Surface Models  
54 (LSMs) does not accurately simulate vegetation carbon dynamics during drought (Sitch *et al.*,  
55 2008; Powell *et al.*, 2013; Medlyn *et al.*, 2016; Ukkola *et al.*, 2016; Restrepo-Coupe *et al.*, 2017;  
56 Rogers *et al.*, 2017; Eller *et al.*, 2018b), thereby restricting our capability to predict the effect of  
57 increased aridity on vegetation distribution and its feedbacks on the global carbon cycle and  
58 climate. Many LSMs represent the effects of reduced soil moisture on canopy carbon assimilation  
59 (A) using an empirical drought factor commonly referred as  $\beta$ -factor (Cox *et al.*, 1998). The  $\beta$ -  
60 factor approach has been shown to overestimate plant responses to seasonal and experimentally  
61 induced drought (Ukkola *et al.*, 2016; Restrepo-Coupe *et al.*, 2017; Eller *et al.*, 2018b). The  $\beta$ -  
62 factor has a large impact on the modelled global carbon budget, suppressing 30-40% of the annual  
63 gross primary productivity (GPP) in large areas of arid and semi-arid ecosystems (Trugman *et al.*,  
64 2018). Despite its importance, there is scarce empirical support for the drought functions used in  
65 most LSMs (Medlyn *et al.*, 2016). The lack of a theoretical or empirical basis for the  $\beta$ -factor  
66 implies an urgent need for new modelling approaches to replace this important component of  
67 LSMs so as to improve our capacity to predict vegetation-climate interactions.

68 Stomatal responses of plants to soil drought involve complex chemical signalling and  
69 hydrodynamic processes in leaf cells, some of which have not been entirely elucidated (Buckley,  
70 2017; 2019; Qu *et al.*, 2019). Stomatal optimization models are a useful approach to model

71 stomatal behaviour that circumvents the need to explicitly represent the physiological processes  
72 involved in stomatal regulation. Optimization models employ a ‘goal-oriented’ approach,  
73 assuming that plant stomata behaviour has been selected through plant evolutionary history to  
74 maximize a given objective function (Cowan, 2002; Dewar *et al.*, 2009; Prentice *et al.* 2014;  
75 Buckley, 2017). The traditional approach to model optimal stomatal behaviour is derived from the  
76 seminal work of Cowan & Farquhar (1977). This approach proposes that optimal stomatal  
77 behaviour maximizes  $A$  minus the carbon cost of water lost ( $\lambda E$ ) over a given time interval, where  
78  $E$  is transpiration and  $\lambda$  is the lagrange multiplier that represents the carbon cost of a unit of water  
79 lost. This model, hereafter labelled CF, after Cowan & Farquhar, is capable of simulating many  
80 patterns of stomatal responses to climate over short time scales (Farquhar *et al.*, 1980; Berninger  
81 & Hari, 1993), and has provided the theoretical basis for several widely used semi-empirical  
82 stomatal models (Jacobs, 1994; Leuning, 1995; Medlyn *et al.*, 2011). However, CF predicts that  
83 stomatal conductance ( $g_s$ ) increases in response to elevated  $\text{CO}_2$  when  $A$  is Rubisco-limited, which  
84 contradicts most observations (Mott, 1988; Medlyn *et al.*, 2001). Other limitations are related to  
85 the  $\lambda$ , as the CF hypothesis does not link  $\lambda$  to measurable plant traits or environmental quantities  
86 (Buckley, 2017), and assumes  $\lambda$  is constant over the period of reference (Cowan & Farquhar,  
87 1977), which makes the original CF unable to predict long-term  $g_s$  decline in response to soil  
88 moisture depletion.

89 Since the original CF work many attempts have been made to incorporate the effects of  
90 declining soil moisture in the CF stomatal optimization framework (Cowan, 1986; Mäkelä *et al.*,  
91 1996; Williams *et al.*, 1996; Manzoni *et al.*, 2013). Some of these attempts, such as the Soil-Plant-  
92 Atmosphere (SPA) model of Williams *et al.* (1996), employ principles of plant hydraulics to  
93 constrain stomatal optimization and have been successfully incorporated into LSMs (Bonan *et al.*,

94 2014). The numerical approach used by SPA employs a hydraulic threshold to set a lower water  
95 potential limit ( $\Psi_{min}$ ) for  $g_s$ , which simulates a strict isohydric stomatal regulation (Fisher *et al.*,  
96 2006). Despite using plant hydraulics SPA still relies on a water-use efficiency optimization  
97 similar to CF to model stomatal behaviour when  $\Psi > \Psi_{min}$  (Williams *et al.*, 1996; Bonan *et al.*,  
98 2014).

99 Alternative routes to model plant optimal stomatal behaviour have been proposed recently (see  
100 Mencuccini *et al.*, 2019a for a review). These approaches circumvent the CF limitations by  
101 assuming plant optimal stomatal behaviour minimizes the instantaneous fitness costs associated  
102 with low  $\Psi$ . These new optimization models use widely available plant hydraulic traits (Kattge *et*  
103 *al.*, 2011; Choat *et al.*, 2012) to simulate  $g_s$  responses to environmental conditions, producing a  
104 realistic  $g_s$  decline in response to elevated atmospheric CO<sub>2</sub> and soil drought (Sperry *et al.*, 2017;  
105 Eller *et al.*, 2018b; Venturas *et al.*, 2018; Wang *et al.*, 2019). This approach predicts a tight  
106 coordination between stomatal and xylem functioning which is widely corroborated by  
107 observations (Hubbard *et al.*, 2001; Meinzer *et al.*, 2009; Klein, 2014). Another advantage of this  
108 approach is its capacity to simulate a diversity of contrasting stomatal behaviours, from iso to  
109 anisohydric (Martinez-Vilalta *et al.*, 2014; Klein, 2014).

110 Sperry *et al.* (2017) proposes a model that assumes that, as xylem hydraulic conductance  
111 declines, the increased risk of hydraulic failure is the main fitness cost associated with low  $\Psi$ . Eller  
112 *et al.* (2018b) adapted the Sperry *et al.* (2017) model into the stomatal optimization model based  
113 on xylem hydraulics (SOX), which principally differs from the Sperry *et al.* (2017) model by using  
114 a different optimization target. The SOX optimization target is based on the PGEN model (Friend,  
115 1995), which assumes stomata optimize plant dry matter production, represented by the product  
116 of photosynthesis and a linear function of  $\Psi$ . The SOX model in Eller *et al.* (2018b) uses a



117 numerical routine to find the optimum  $g_s$ . However, the PGEN optimization target can also be  
 118 found analytically (Friend & Cox, 1995; Dewar *et al.*, 2018). A parsimonious analytical  
 119 formulation for SOX would facilitate its incorporation into existing LSMs and provide a practical  
 120 alternative to the  $\beta$ -function for modelling stomatal responses to drought at global scales.

121 In this study we develop an analytical approximation for the numerical SOX model presented  
 122 in Eller *et al.* (2018b). We then create a new configuration for the Joint UK Land Environment  
 123 Simulator (JULES; Best *et al.*, 2011; Clark *et al.*, 2011) that uses SOX to compute vegetation  $g_s$   
 124 from environmental and plant hydraulic data. Using a global dataset of xylem hydraulic traits,  
 125 together with an extensive leaf gas-exchange and eddy covariance dataset, we calibrate the SOX  
 126 parameters and compare the JULES-SOX performance to the default JULES using the  $\beta$ -function,  
 127 across all major global biomes. Our goals in this paper are twofold: 1- To test SOX agreement  
 128 with global observations of  $g_s$  to assess the generality of the underlying hypothesis in SOX, that  
 129 is, that plant stomata evolved to balance carbon assimilation with the loss of hydraulic  
 130 conductance; and 2 – To evaluate the effect of SOX on JULES ecosystem-scale predictions of  
 131 carbon and water fluxes, and their agreement with observations.

## 132 **Materials and Methods**

### 133 *Analytical SOX description*

134 The SOX central hypothesis can be summarised as ‘*stomatal conductance ( $g_s$ ) is such as to*  
 135 *maximise the product of leaf photosynthesis and xylem hydraulic conductance*’ and given by:

$$136 \quad A(c_i(g_s)) K(\Psi_m(g_s)) \quad (\text{Eqn 1})$$

137 where  $A$  is leaf net CO<sub>2</sub> assimilation (mol CO<sub>2</sub> m<sup>-2</sup> s<sup>-1</sup>), which is a function of leaf internal CO<sub>2</sub>  
 138 partial pressure ( $c_i$ ; Pa), which is itself a function of stomatal conductance to CO<sub>2</sub> ( $g_s$ ; mol m<sup>-2</sup> s<sup>-1</sup>).  
 139 The  $K$  is the normalised (0 to 1) xylem hydraulic conductance computed as:

$$140 \quad K(\Psi) = \frac{1}{[1 + (\Psi/\Psi_{50})^a]} \quad (\text{Eqn 2})$$

141 where  $\Psi_{50}$  is  $\Psi$  when  $K = 0.5$  and the parameter  $a$  gives the shape of the curve, with a higher  $a$   
 142 producing a steeper response to  $\Psi$ . We use the mean ( $\Psi_m$ ; MPa) of the canopy water potential at  
 143 the predawn ( $\Psi_{pd}$ ; MPa) and the canopy water potential ( $\Psi_c$ ; MPa) to compute  $K$  with equation 2  
 144 to account for the gradual decline in  $\Psi$  along the soil to canopy hydraulic pathway (see details in  
 145 Notes S1). The  $g_s$  value that maximises equation 1 is found at:

$$146 \quad \frac{\partial AK}{\partial g_s} = 0 \quad (\text{Eqn 3})$$

147 The  $g_s$  value that satisfies equation 3 was found numerically in Eller *et al.* (2018b), but a  
 148 computationally efficient analytical solution is preferable for application in Dynamic Global  
 149 Vegetation Models (DGVMs) and ESMs. We developed an analytical approximation for the  
 150 optimal SOX  $g_s$  using the partial derivatives of  $A$  with respect to  $c_i$  and  $K$  with respect to  $\Psi_m$ . All  
 151 steps of the model derivation are described in Notes S1. The resulting SOX equation for the  
 152 optimal  $g_s$  is:

$$153 \quad g_s = 0.5 \frac{\partial A}{\partial c_i} \left( \sqrt{\frac{4\xi}{\partial A / \partial c_i} + 1} - 1 \right) \quad (\text{Eqn 4})$$

154 The benefit of stomatal opening is represented here by the sensitivity of leaf photosynthesis to the  
 155 internal CO<sub>2</sub> concentration ( $\partial A / \partial c_i$ ). By contrast, the parameter  $\xi$  represents the cost of stomatal  
 156 opening in terms of loss of xylem conductivity under low  $\Psi_{pd}$  and/or higher leaf-to-air vapour  
 157 pressure ( $D$ ; mol mol<sup>-1</sup>):

$$158 \quad \xi = \frac{2}{1/K \partial K / \partial \Psi_m r_p 1.6D} \quad (\text{Eqn 5})$$

159 Low  $\xi$  indicates high hydraulic costs occurring during drought (i.e. lower  $\Psi_{pd}$  and higher  $D$ , Fig.  
 160 S1). SOX simulates dynamic changes on the plant hydraulic resistance ( $r_p$ ) computing  $r_p$  as a  
 161 function of  $\Psi_{pd}$  and the plant minimum hydraulic resistance ( $r_{p,min}$ ,  $\text{m}^2 \text{ s MPa mol}^{-1} \text{ H}_2\text{O}$ ):

$$162 \quad r_p = \frac{r_{p,min}}{K(\Psi_{pd})} \quad (\text{Eqn 6})$$

163 Solving SOX main equations (Eqn 4-5) requires computing the partial derivatives of  $A$  and  $K$ ,  
 164  $\partial A/\partial c_i$  and  $\partial K/\partial \Psi_m$ , respectively. These derivatives were estimated numerically in this study as  
 165 described in Notes S2.

166 We evaluated SOX as a stand-alone leaf-level model, and coupled to JULES, hereafter JULES-  
 167 SOX. The leaf-level model was evaluated against leaf gas exchange data as an ‘assumption  
 168 centred’ (*sensu* Medlyn *et al.*, 2015) test of the hypothesis underlying SOX. The JULES-SOX was  
 169 then evaluated against ecosystem-level eddy flux data, which constituted the first practical test of  
 170 the utility of SOX for LSMs.

#### 171 *JULES $\beta$ -function description*

172 The JULES model (Best *et al.*, 2011; Clark *et al.*, 2011) uses the Collatz *et al.* (1991, 1992)  
 173 photosynthesis model for  $C_3$  and  $C_4$  plants (Notes S3) to produce unstressed rates of  $A$  based on  
 174 the co-limitation of light, Rubisco carboxylation capacity, and the transport of photoassimilates  
 175 (for  $C_3$  plants) and PEPcarboxylase limitation (for  $C_4$  plants). The effect of soil moisture in  $A$  in  
 176 the default JULES is given by multiplying  $A$  by the  $\beta$  factor, computed using the  $\beta$ -function from  
 177 Cox *et al* (1998):

$$178 \quad \beta = \begin{cases} 1 & \text{for } \theta > \theta_c \\ \frac{\theta - \theta_w}{\theta_c - \theta_w} & \text{for } \theta_w < \theta \leq \theta_c \\ 0 & \text{for } \theta \leq \theta_w \end{cases} \quad (\text{Eqn 7})$$

179 where  $\theta$  is the mean soil moisture in the root zone ( $\text{m}^3 \text{m}^{-3}$ ), and  $\theta_c$  and  $\theta_w$ , are the critical and  
 180 wilting points, which are defined by Cox *et al.* (1998) as the  $\theta$  when soil  $\Psi$  is -0.033 and -1.5 MPa,  
 181 respectively. The default JULES formulation employs the Jacobs (1994) equation to predict  $c_i$  from  
 182  $D$ ,  $c_a$  and the  $\text{CO}_2$  compensation point,  $\Gamma$  (Pa):

$$183 \quad c_i = f_0 \left( 1 - \frac{D}{D_{crit}} \right) (c_a - \Gamma) + \Gamma \quad (\text{Eqn 8})$$

184 where  $f_0$  and  $D_{crit}$  are empirical parameters (Jacobs, 1994; Cox *et al.*, 1998).

185 The JULES-SOX configuration replaces equations 7-8, computing  $g_s$  from environmental data  
 186 and plant hydraulic inputs with equations 4-5. To compute  $A$  from the  $g_s$  predicted by equation 4,  
 187 we solved the limiting photosynthetic rates from the Collatz *et al.* (1991; 1992) model as functions  
 188 of  $c_a$  and  $g_s$ , as described in Notes S3.

### 189 *Leaf-level SOX evaluation*

190 We used a global compilation of leaf gas exchange data to evaluate the SOX capacity to  
 191 reproduce leaf stomatal responses of a wide range of woody plants. This dataset contains  
 192 observations compiled by Lin *et al.* (2015), complemented with other published and unpublished  
 193 data (see Table S1 and Fig. S2 for additional information). In total, there are 3597 measurements  
 194 of  $g_s$  and  $\Psi_{pd}$  together with environmental variables used for driving the model, that is: incident  
 195 photosynthetic active radiation ( $I_{par}$ ), air temperature ( $T_a$ ),  $c_a$  and  $D$ . This data comes from 30  
 196 woody plant species collected in 15 sites around the world (Fig. S2b). The  $\Psi_{pd}$  was measured on  
 197 the same day as  $g_s$ , and the environmental data was measured simultaneously with  $g_s$ . The dataset  
 198 included field and greenhouse observations, with environmental conditions varying from well-  
 199 watered to extreme drought ( $\Psi_{pd} = -7$  MPa). These observations were grouped into the global Plant  
 200 Functional Type (PFT) categories from Harper *et al.* (2016) (Table 1). Harper *et al.* (2016) divides  
 201 Angiosperms tree species into Broadleaved Evergreen Tropical Trees (BET-Tr), Broadleaved

202 Evergreen Temperate Trees (BET-Te) and Broadleaved Deciduous Trees (BDT), while  
203 Gymnosperms tree species are divided into Needle-leaved Evergreen Trees (NET) and Needle-  
204 leaved Deciduous Trees (NDT). Shrub species were divided into Evergreen Shrubs (ESh) and  
205 Deciduous Shrubs (DSh), and two grass PFTs defined by their photosynthetic pathway ( $C_3$  and  
206  $C_4$ ). The grass PFTs and the NDT were excluded from the leaf-level evaluation because no  
207 stomatal conductance data were available for these PFTs in the dataset used in this study.

208 The plant hydraulic parameters used in SOX (i.e.  $\Psi_{50}$ ,  $a$ , and  $r_{pmin}$ ) were fitted to the  $g_s$  data  
209 using an algorithm that minimizes the model residual sum of squares within the constraints of the  
210 observed  $\Psi_{50}$ ,  $a$  and  $r_{pmin}$ . We compiled hydraulic data for each PFT from the literature to constrain  
211 the leaf-level model fit. The  $\Psi_{50}$  for woody plants was obtained from a version of the Choat *et al.*  
212 (2012) dataset updated recently by Mencuccini *et al.* (2019b). The shape parameter  $a$  of the xylem  
213 vulnerability function (Eqn 2) was estimated from the linear gradient between  $\Psi_{50}$  and the  $\Psi$  when  
214 the plant loses 88% of its maximum hydraulic conductance. The  $r_{pmin}$  was estimated from branch-  
215 level hydraulic conductivity measurements scaled from branch to whole plant taking into account  
216 plant height, Huber value and xylem tapering using the calculations described in Christoffersen *et al.*  
217 (2016) and Savage *et al.* (2010) (Notes S4). All the data used for these calculations were  
218 obtained from the hydraulic dataset from Mencuccini *et al.* (2019b). We note that scaling branch  
219 to whole tree  $r_{pmin}$  requires several assumptions about tree hydraulic architecture (Notes S4).  
220 Therefore, the presented values of  $r_{pmin}$  must be considered as a reference useful only to assess if  
221 the  $r_{pmin}$  input values used in the model are within the same order of magnitude of the observations.  
222 The other parameters of the photosynthesis model used in SOX (Notes S3) were set equal to Harper  
223 *et al.* (2016).

224 The model predictive skill was evaluated using the model root mean squared errors (RMSE)  
225 and the Nash and Sutcliffe (1970) model efficiency index (NSE). The NSE varies from  $-\infty$  to 1,  
226 with 1 indicating perfect agreement between model and observations, while  $NSE < 0$  indicates the  
227 mean value of the observations is a better predictor than the model. The model parsimony was  
228 evaluated using the Akaike Information Criterion (AIC), which penalizes model  
229 overparameterization (Bozdogan, 1987). We compared SOX AIC score with the  $\beta$ -function (Eqn  
230 7-8). The parameters  $f_0$  and  $D_{crit}$ , (Eqn 8) were fitted to the PFT  $g_s$  data, while the  $\theta_c$  and  $\theta_w$  were  
231 held at their default values (-0.033 and -1.5 MPa, respectively).

232 The uncertainty in plant hydraulic parameters caused by within PFT hydraulic variability was  
233 propagated to the model predictions using bootstrapped 95% confidence intervals. We created the  
234 interval based on 1000 model runs with parameters resampled from the hydraulic trait data for  
235 each PFT.

#### 236 *Eddy-covariance based JULES-SOX evaluation*

237 We evaluated default JULES and JULES-SOX against daily gross primary productivity (GPP)  
238 estimates derived from eddy flux tower data at 62 FLUXNET sites (<http://fluxnet.fluxdata.org>,  
239 Baldocchi *et al.*, 2001) and 8 LBA sites (<https://daac.ornl.gov/LBA>, Saleska *et al.*, 2013) covering  
240 all the major biomes of the world (Fig. S2, Table S2). In 10 of these sites we also had data for  
241 surface (5 to 15 cm) soil moisture content, which was used to evaluate the model soil moisture  
242 dynamics predictions. We classified the land cover on each site using the International Geosphere-  
243 Biosphere Programme (IGBP) classification (Loveland *et al.*, 2000). Each site was classified as  
244 one of the following categories according to its prescribed PFT cover (Table S2): cropland (CRO),  
245 deciduous broadleaf forests (DBF), deciduous needleleaf forests (DNF), temperate evergreen  
246 broadleaf forests (EBF-Te), tropical evergreen broadleaf forests (EBF-Tr), evergreen needleleaf

247 forest (ENF), grassland (GRA), mixed forest (MF), savannah (SAV), shrubland (SHR), and  
248 wetlands (WET). We grouped the IGBP categories open and closed shrublands into SHR, as we  
249 only had a single closed shrubland site. Similarly, woody savannah was grouped with SAV, as we  
250 only had two woody savannah sites. We divided the evergreen broad leaf forests category into  
251 EBF-Te and EBF-Tr, as these sites were dominated by distinct PFTs (BET-Te and BET-Tr,  
252 respectively).

253 We evaluated JULES-SOX using the SOX hydraulic parameters (i.e.  $\Psi_{50}$ ,  $a$ , and  $r_{pmin}$ ) that  
254 minimized the residual sum of squares between SOX predictions and the eddy flux GPP  
255 observations from a subset of the sites used for model evaluation (Fig. S2; Table S2). Each site  
256 was used to calibrate the hydraulic parameters for its dominant PFT (i.e. the PFT covering more  
257 than 50% of the site area), except for DSh, which was not dominant in any of the available sites.  
258 We used a site with DSh cover of 35% (US-SRM) to calibrate the hydraulic parameters of this  
259 PFT. The hydraulic parameters of the others PFTs (if any) present on the site were kept constant  
260 during the model runs for parameter calibration. Similar to the leaf-level evaluation, the parameter  
261 calibration in JULES-SOX was constrained within the range of the observed values of  $\Psi_{50}$ ,  $a$ , and  
262  $r_{pmin}$  for all PFTs, except NDT which did not have enough observations to satisfactorily constrain  
263 the model parameters. The  $\Psi_{50}$  for grasses was obtained from Lens *et al.* (2016) dataset updated  
264 with data from Ocheltree *et al.* (2016).

### 265 *Model setup*

266 The JULES and JULES-SOX configuration used in this study employed the 10-layer canopy  
267 scheme with sunlit and shaded leaves in each layer as described in Clark *et al.* (2011). The canopy  
268 radiation profile was given by the two-stream approach from Sellers (1985), with the sun-fleck  
269 penetration scheme from Mercado *et al.* (2009), and an exponential decrease of photosynthetic

270 capacity through the canopy (Mercado *et al.*, 2007). All the model runs used in this study were  
 271 site-level simulations driven with hourly local meteorological data. Vegetation dynamics (Cox,  
 272 2001) was turned off and the site PFT coverage by site was prescribed based on the site vegetation  
 273 description obtained from the site principal investigators (Table S3) or information from the site  
 274 available on the FLUXNET website (<https://fluxnet.fluxdata.org/sites/site-list-and-pages/>). Site  
 275 soil hydraulic properties were parameterised using Brooks and Corey (1964) relations. These  
 276 properties were derived from data collected at each site or, when local data were not available,  
 277 calculated from the sand/silt/clay fractions in the nearest gridbox in the high-resolution input file  
 278 to the Met Office Central Ancillary Program (Dharssi *et al.*, 2009), using approximations from  
 279 Cosby *et al.* (1984). The model was spun-up by recycling the meteorological data at each site for  
 280 up to 50 years.

## 281 **Results**

### 282 *SOX sensitivity to environmental and hydraulic drivers*

283 The SOX analytical approximation (Eqn 4-5) has  $g_s$  responses to climate which are consistent  
 284 with the patterns commonly reported in the literature (Mott, 1988; Leuning, 1995; Dewar *et al.*,  
 285 2018). The  $g_s$  responses to  $I_{\text{par}}$  and  $c_a$  in SOX (Fig. 1a) are given by the  $\partial A/\partial c_i$  gradient decreasing  
 286 at low light because of the changes in the light response curve, as  $A$  starts being limited by light  
 287 (Notes S3), or at high  $c_a$ , which affects the gradient between  $A(c_a)$  and  $A(c_{i,\text{col}})$  (Notes S2). SOX  
 288 correctly predicted stomatal closure in response to increased  $c_a$  under Rubisco-limited conditions  
 289 (Mott, 1988; Fig. 1a). The classical exponential  $g_s$  responses to  $D$  (Leuning, 1995) was reproduced  
 290 in SOX (Fig. 1a) through the  $D$  effect on  $\xi$  (Eqn 5; Fig. S1a). An exponential  $g_s$  decline was also  
 291 predicted by SOX in response to decreasing  $\Psi_{pd}$ , (Fig. 1a) which summarizes both the responses  
 292 to the soil water availability in the root zone and the hydraulic stress of transporting water to the



293 top of the canopy (Eqn S1.2 in Notes S1). The plant hydraulic parameters modulated the model  
 294 sensitivity to  $D$  or  $\Psi_{pd}$  (Fig. 1b-d), with a less negative  $\Psi_{50}$  or a higher  $r_{pmin}$  increasing the  $g_s$   
 295 sensitivity to  $\Psi_{pd}$  and  $D$  (Fig. 1c-d). The effect of the vulnerability curve shape parameter  $a$  was  
 296 more complex, lower  $a$  increased  $g_s$  sensitivity to less negative  $\Psi_{pd}$ , but decreased  $g_s$  sensitivity to  
 297 very negative  $\Psi_{pd}$  values (Fig. 1c).

298 The patterns produced by the analytical SOX were similar to the numerical version from Eller  
 299 *et al.* (2018b), with a correlation coefficient ranging from 0.92 to 1 (Fig. S3). However, the use of  
 300 linear gradients in equations 4 and 5 (Notes S2) can cause discrepancies between the different  
 301 model versions under certain ranges of environmental conditions. The analytical version of SOX  
 302 underestimated  $g_s$  at low  $D$  (Fig. S3), overestimated  $g_s$  at low  $c_a$ , and  $g_s$  increased faster in response  
 303 to light (Fig. S3) than in the numerical model.

#### 304 *SOX leaf-level evaluation*

305 SOX simulated the observed leaf-level  $g_s$  responses to soil drought better than the  $\beta$ -function  
 306 in all the studied woody PFTs, except BDT (Fig. 2). The  $\beta$ -function predicted all PFTs will reach  
 307  $g_s = 0$  at  $\Psi_{pd} > -2$  MPa, whereas SOX predicted  $g_s > 0$  even when  $\Psi_{pd} < -4$  MPa in some PFTs (Fig.  
 308 2b, e). The less conservative stomatal behaviour predicted by SOX produced a NSE, on average,  
 309 0.65 higher and a RMSE 26% lower than the  $\beta$ -function. Most of the observed  $g_s$  was within SOX  
 310 95% confidence bounds derived from the hydraulic parameters' uncertainty (shaded region in Fig.  
 311 2). The only values outside SOX uncertainty boundaries were the highest  $g_s$  values in BET-Tr and  
 312 BET-Te (Fig. 2a-b), and the lowest NET  $g_s$  values when  $\Psi_{pd} > -3.5$  MPa (Fig. 2d).

313 SOX produced a better fit to the  $g_s$  data, which resulted in a lower AIC than the  $\beta$ -function for  
 314 all PFTs, except BDT (Table 1). Fitting the two empirical parameters of the Jacobs (1994) equation  
 315 ( $f_0$  and  $D_{crit}$ , Eqn 8) to the  $g_s$  data results in a  $\beta$ -function AIC score 512.1 higher than SOX (Table

316 1). For the BDT observations, the  $\beta$ -function results in an AIC score 11.6 lower than SOX. Our  
 317 BDT observations were restricted to relatively well watered conditions (lowest  $\Psi_{pd}$  was -1.2 MPa),  
 318 which limits the utility of this dataset to evaluate the model responses to soil drought.

### 319 *JULES-SOX site-level calibration*

320 The hydraulic parameters that maximized the JULES-SOX fit to the GPP data at the calibration  
 321 sites (Table S2; Fig. S2) were within one SD of the mean observed hydraulic parameters for most  
 322 PFTs (Table 2). The Gymnosperm PFTs (NDT and NET) required  $\Psi_{50}$  values 1.6 MPa less  
 323 negative than their observed  $\Psi_{50}$  means to fit the GPP data, which is lower than the observed SD  
 324 range but still within the range of  $\Psi_{50}$  observations for NET ( $\Psi_{50}$  ranges from -2.3 to -7.5 MPa in  
 325 NET). The NDT and BET-Tr calibrated  $a$  were also slightly lower than the SD range (Table 2),  
 326 but within the observed  $a$  range for BET-Tr ( $a$  ranges from 1.8 to 7.8 in BET-Tr). The only PFT  
 327 with a calibrated  $r_{pmin}$  outside the SD range of the mean  $r_{pmin}$  was ESh (Table 2).

328 The monthly GPP modelled by JULES-SOX fitted the eddy covariance GPP data better than  
 329 the default JULES in 8 out of the 9 sites used for parameter calibration (Table S2; Fig. S2) (Fig.  
 330 3). The default JULES NSE was 0.01 higher in the DSh site (Fig. 3i), whereas in all the other sites  
 331 JULES-SOX had a better fit. The difference between JULES-SOX and default JULES NSE ranged  
 332 from 0.03 for C3 grasses (Fig. 3f) to 11.44 for BET-Tr (Fig. 3a). The large improvement in the  
 333 BET-Tr site was caused by the lower GPP decline predicted by SOX during Jan-Mar and Sep-Dec.  
 334 The decline in BET-Tr GPP in default JULES can be attributed to the  $\beta$ -factor overestimating the  
 335 effects of soil moisture on the vegetation carbon assimilation during drier periods (Fig. S4a). On  
 336 average, JULES-SOX NSE for GPP was 1.59 higher than default JULES, while its RMSE was  
 337 38% lower than JULES.

338 The less conservative stomatal behaviour predicted by SOX resulted in higher  
339 evapotranspiration rates throughout the year (Fig. S5; S6), which depleted soil moisture to lower  
340 levels than the  $\beta$ -function in default JULES during drier periods (Fig. S4; S7). The soil moisture  
341 dynamics from JULES-SOX are more closely aligned with the monthly soil moisture observations  
342 in 8 out of the 10 sites where soil moisture data was available (Fig. S7). JULES-SOX NSE for  
343 monthly soil moisture was 1.67 higher and a RMSE 19% lower than default JULES. JULES-SOX  
344 also simulates realistic  $\Psi_c$  for most PFTs (Fig. 4; S4). The modelled  $\Psi_c$  at the calibration sites is  
345 within the interquartile range of the observed minimum  $\Psi_c$  at midday for all woody PFTs, except  
346 NDT (Fig. 4).

#### 347 *Biome-level JULES-SOX evaluation*

348 Using JULES-SOX with calibrated SOX hydraulic parameters produced a better fit to the GPP  
349 data than default JULES for 50 out of the 70 eddy flux evaluation sites (Table S2; Table 3; Fig.  
350 5). Across all biomes the JULES-SOX median NSE was 0.19 higher than default JULES, and its  
351 RMSE was 19% lower (Table 3). The difference between JULES-SOX and JULES skill was  
352 highest at EBF-Tr sites, which have a median NSE 3.18 higher and RMSE 45% lower in JULES-  
353 SOX (Table 3; Fig 5a). The fit of EBT-Te to data was also improved substantially by JULES-  
354 SOX, with JULES-SOX having a median NSE 1.01 higher and a RMSE 18% lower (Fig. 5a; Table  
355 3). Default JULES only outperformed JULES-SOX at CRO, which have a median NSE 0.08 lower  
356 in JULES-SOX, and GRA where the RMSE 5% was higher in JULES-SOX (Fig. 5a; Table 3).

357 Default JULES significantly underestimated the observed mean annual GPP by 143.3 g C m<sup>-2</sup>  
358 across all biomes, which corresponds to 13.6% of the observed mean annual GPP (Fig. 5b).  
359 JULES-SOX deviation from the observed mean annual GPP was considerably smaller (71.6 g C  
360 m<sup>-2</sup>; Fig. 5b). The significantly lower annual GPP predicted by default JULES can be attributed to

361  $\beta$ -function induced GPP declines, which also produced a stronger GPP seasonality than what is  
362 present in the data (Fig. 5c). JULES overestimated the median observed GPP seasonality by 70%,  
363 versus a 13% overestimation by JULES-SOX (Fig. 5c). This difference means JULES predicts  
364 17% of the sites have a markedly seasonal GPP (SI > 0.8; Walsh & Lawler, 1981) while just 4 %  
365 of the sites actually have SI > 0.8. JULES-SOX predicts only 8% of the sites would have SI > 0.8.

366 The light use efficiency (LUE; Fig. 6) is the ratio between GPP and the  $I_{par}$  absorbed by the  
367 canopy (Stocker *et al.*, 2018), and can be used to disentangle the effects of soil moisture and light  
368 availability controlling the vegetation GPP. The JULES LUE declined as soil dries out with a mean  
369 linear slope of 1.21 ( $\pm 0.1$ ) across all biomes. In contrast, the JULES-SOX LUE-soil moisture  
370 relationship had a mean slope of 0.73 ( $\pm 0.21$ ) with some biomes, such as DBF, reaching a slope  
371 as low as 0.22 (Fig. 6b). The consequence of sustaining higher LUE at low soil moisture in JULES-  
372 SOX is a greater depletion of soil moisture, as indicated by the more left skewed soil moisture  
373 probability distribution predicted by JULES-SOX (lower panels in Fig. 6). The mean moisture  
374 content of the top 1 m of soil predicted by JULES-SOX was, on average, 10% lower than default  
375 JULES. In JULES-SOX some biomes, such as ENF, could reach a soil moisture on average 17%  
376 lower than JULES (Fig. 6f).

## 377 Discussion

378 We report the first evaluation of a LSM using a stomatal optimization model fully based on  
379 xylem hydraulics (SOX) to drive the vegetation stomatal responses to climate. Our results provide  
380 support for the SOX underlying hypothesis that stomata evolved to balance carbon assimilation  
381 with instantaneous hydraulic conductance loss. The risk of mortality through hydraulic failure  
382 (Choat *et al.*, 2012; Rowland *et al.*, 2015; Anderegg *et al.*, 2016; Adams *et al.*, 2017), should drive  
383 the evolution of mechanisms to prevent the plant from reaching lethal embolism thresholds

384 (Sperry, 2004). There is abundant evidence that stomata controls xylem tension, and consequently  
385 embolism (Hubbard *et al.*, 2001; Brodribb *et al.*, 2003; Meinzer *et al.*, 2009; Klein, 2014). Our  
386 model represents this xylem-stomata coordination through the assumption of optimisation by  
387 natural selection (Wolf *et al.*, 2016).

388 Whereas our model fits the observations of most PFTs better than its empirical alternative,  
389 there is still a considerable amount of unexplained variance in the data (Fig. 2). This can be  
390 partially attributed to the large hydraulic heterogeneity within each PFT, but we must also  
391 acknowledge that many processes not directly related with xylem hydraulics are important to plant  
392 life history and stomatal evolution. Processes related to nutrient use and acquisition, carbohydrate  
393 allocation and storage, the maintenance of tissues and biochemical apparatus, and protection from  
394 pathogens and herbivores (Melotto *et al.*, 2008; Cramer *et al.*, 2009; Prentice *et al.*, 2014) all could  
395 explain part of our model residual variance. It is extremely important to explore the relevance of  
396 these processes in future research on stomatal optimality. However, the SOX model as we propose  
397 already provides a parsimonious alternative to the empirical models commonly used in LSM.

398 Our findings that xylem hydraulics-based models can adequately simulate stomatal behaviour  
399 agree with other recent studies. For example, Anderegg *et al.* (2018b) shows that a hydraulics  
400 based optimization model can simulate the stomatal behaviour of woody plants better than CF.  
401 More recently, Wang *et al.* (2019) shows that a similar hydraulics-based model can predict  
402 stomatal responses to increased CO<sub>2</sub> better than the Ball-Berry-Leuning empirical model (Leuning,  
403 1995). These results show the potential of using plant hydraulics to model the stomatal behaviour  
404 of plants across contrasting environmental conditions, and supports its use in ESMs to project the  
405 evolution of global climate.

406 The analytical formulation developed for SOX facilitates its coupling to LSMs, allowing the  
407 host LSM to constrain its predictions using plant hydraulic information. We show that including  
408 plant hydraulics in JULES through SOX improves its capabilities to simulate GPP and soil  
409 moisture dynamics in most of the studied biomes (Fig. 3-5). In addition, SOX opens new  
410 possibilities to evaluate LSM predictions and expands the range of hypotheses that can be tested  
411 with JULES. Using JULES-SOX within ESMs will allow us to understand how hydraulic  
412 processes affect climatic and biogeochemical cycles at global scale, as well as to investigate the  
413 role of plant hydraulics on vegetation distribution and its response to climate change.

#### 414 *SOX parametrization and parsimony*

415 Other LSMs and DGVMs have already successfully employed principles of plant hydraulics  
416 (Hickler *et al.*, 2006; Bonan *et al.*, 2014; Kennedy *et al.*, 2019), but JULES-SOX is the first LSM  
417 to use the new generation of hydraulically-based stomatal optimization models (Wolf *et al.*, 2016;  
418 Sperry *et al.*, 2017; Anderegg *et al.*, 2018b; Eller *et al.*, 2018b) to predict stomatal responses to  
419 climate. The SPA (Williams *et al.*, 1996) adaptation to the Community Land Model (CLM) by  
420 Bonan *et al.* (2014) was one of the first approaches to link plant stomatal function to plant hydraulic  
421 processes in a LSM. Despite SPA being an extremely useful model, SOX has an advantage in  
422 circumstances where assuming a strict isohydric behaviour is not appropriate (Klein, 2014;  
423 Martinez-Vilalta *et al.*, 2014). In relation to SOX, SPA does not represent dynamic changes in the  
424 plant hydraulic conductance or an anisohydric mode of stomatal regulation (Williams *et al.*, 1996;  
425 Fisher *et al.*, 2006). However, SPA accounts for plant hydraulic capacitance, which can be  
426 important for plant functioning, especially during early morning (Goldstein *et al.*, 1998), and is  
427 currently not implemented in SOX.

428 Recently Kennedy *et al.* (2019) implemented a Plant Hydraulic Scheme (PHS) in CLM. The  
429 PHS simulates dynamic changes in hydraulic conductance in different compartments along the  
430 soil-atmosphere continuum, providing a more detailed representation than SOX of hydraulic  
431 processes occurring along the soil-plant hydraulic pathway. However, PHS still requires empirical  
432 parameters to represent stomatal responses to soil drought and  $D$  (Kennedy *et al.* 2019), namely  
433 the  $g_0$  and  $g_l$  parameters from the Medlyn *et al.* (2011) model, and the critical and wilting points  
434 used in the empirical stress factor. The main advantage of SOX is providing an alternative to the  
435  $\beta$ -function and empirical stomatal parameters by linking plant hydraulic processes directly to  
436 stomatal functioning. As we treat the soil-plant-atmosphere pathway as a single hydraulic  
437 compartment, SOX only requires the hydraulic parameters  $r_{pmin}$ ,  $\Psi_{50}$  and  $a$  to predict stomatal  
438 responses to climate. This makes SOX even more parsimonious than default JULES, which  
439 requires four empirical parameters to simulate stomatal responses to climate (Eqn 7-8) and does  
440 not simulate any aspect of vegetation hydraulic functioning (Clark *et al.*, 2011).

441 We show that the SOX hydraulic parameters in most PFTs can be constrained with plant  
442 branch-level hydraulic observations (Table 2), which is an advantage over models that employ  
443 empirical parameters difficult to constrain and interpret biologically. However, we observed  
444 discrepancies between the SOX-calibrated parameters and the observed hydraulic traits in certain  
445 PFTs (Table 2). In some cases, such as NDT, the parameter discrepancy may have been due to a  
446 very restricted observational sampling of hydraulic parameters in this group. The NDT only had  
447  $\Psi_{50}$  data for five species and  $a$  and  $r_{pmin}$  for two species (Table 2). Considering that the observations  
448 used in this study were not collected in the same FLUXNET sites used to evaluate SOX, some of  
449 the observed discrepancies between calibrated and measured parameters might reflect hydraulic  
450 differences between populations treated as the same PFT in this study. For example, the deciduous

451 angiosperms species present in the XFT dataset used in this study contain mostly hydraulic data  
452 from cold-deciduous temperate species (Mencuccini *et al.*, 2019b), which might not be adequate  
453 to describe the hydraulic system of tropical and subtropical drought-deciduous. Our hydraulic  
454 scheme opens possibilities to improve the representation of different global vegetation types in  
455 JULES with different hydraulic and phenological strategies. Capturing the large diversity of  
456 ecological strategies in plants is important to simulate species rich ecosystems such as tropical  
457 forests (Xu *et al.*, 2016).

458 Anderegg *et al.* (2018a) computed the community weighted average values for  $\Psi_{50}$  in two of  
459 the FLUXNET sites used in this study (US-MMS and IT-Ren) and obtained values closer to the  
460 calibrated values for BDT and NET (-2.1 and -3.6 MPa, respectively), than the means from our  
461 compiled hydraulic dataset (Table 2). In Eller *et al.* (2018b) a numerical version of SOX  
462 outperformed the  $\beta$ -function approach when parameterized with locally measured branch-level  
463 hydraulic data from EBF-Tr. These findings suggest that SOX can be constrained with *in-situ*  
464 hydraulic measurements when these are available. However, we must also consider the possibility  
465 that there are intrinsic limitations in using branch-level hydraulic data to parameterize the model.  
466 Roots and leaves can be more vulnerable to embolism than branches (Bartlett *et al.*, 2016; Wolfe  
467 *et al.*, 2016), which can make these tissues bottleneck plant hydraulic conductance during drought.  
468 The soil outside the roots can also limit plant hydraulic conductance and, ultimately, control its  
469 water use (Fisher *et al.* 2007). These bottlenecks could bias the SOX calibrated hydraulic  
470 parameters towards the limiting component and explain its departure from the branch-level  
471 hydraulic data. In this case SOX parameterization would benefit from the use of more integrative  
472 methodologies to estimate hydraulic parameters that represent the entire soil-plant hydraulic  
473 vulnerability (Eller *et al.*, 2018a). Alternatively, the SOX structure (i.e., the  $K$  function in Eqn 2)



474 would need to explicitly represent the variability between different hydraulic compartments along  
475 the soil-plant-atmosphere pathway, similarly to SPA or other models (Kennedy *et al.*, 2019;  
476 Mencuccini *et al.*, 2019b; Eller *et al.*, 2018b).

#### 477 *Ecosystem-level implications of SOX*

478 SOX improved JULES GPP simulation in over 70% of the 70 studied sites and soil moisture  
479 dynamics in 80% of the 10 sites where soil moisture data were available. This improved fit was  
480 achieved using hydraulic parameters calibrated against the GPP data of a small subset of eddy flux  
481 sites (the sites in Fig. S2), which suggests that the calibrated parameters are generic enough to be  
482 used in global simulations. The lower sensitivity of SOX to soil moisture improved the simulations  
483 of annual GPP (Fig. 5) and predicted terrestrial biomes to assimilate on average 2.58 Mg C ha<sup>-1</sup>  
484 yr<sup>-1</sup> or 30% more than predicted by default JULES. This increased carbon assimilation could affect  
485 Earth's atmospheric CO<sub>2</sub> evolution and climate change projections (Cox *et al.*, 2000; Winkler *et*  
486 *al.*, 2019) .

487 JULES-SOX particularly improved the fit of EBF-Tr sites to the observations (Fig. 5; Table  
488 3), using hydraulic parameters very similar to those observed in BET-Tr (Table 2). Considering  
489 that SOX is also able to capture the response of EBF-Tr even to extreme experimental drought  
490 (Eller *et al.*, 2018b), JULES-SOX may contribute to decrease the large uncertainty in how these  
491 important ecosystems will respond to climate change (Sitch *et al.*, 2008). Tropical forest  
492 productivity estimated by SOX is less sensitive to seasonal soil drought (Fig. 3; S4), which is  
493 consistent with the little seasonality often observed in tropical forest-atmosphere CO<sub>2</sub> exchange  
494 (Grace *et al.*, 1995; Carswell *et al.*, 2002; Alden *et al.*, 2016), as well as to forest responses to  
495 experimental drought (Meir *et al.*, 2009; da Costa *et al.*, 2010; Meir *et al.*, 2018). da Costa *et al.*  
496 (2018) shows that even after 15 years of partial rainfall exclusion, Amazon trees can maintain or

497 even increase their transpiration rates (albeit following significant mortality). Whereas tropical  
498 forest resistance to drought has previously been attributed only to deep roots possessed by the  
499 vegetation (Nepstad *et al.*, 1994), our results indicate that plants more resistant to embolism could  
500 maintain their carbon assimilation during drought even without a deeper root system.

501 The unavoidable consequence of maintaining stomatal gas exchange during soil drought is a  
502 greater depletion of soil moisture reserves (Fig. 6; S4; S7). This behaviour is a direct consequence  
503 of the main assumption in SOX, which reflects a ‘use or lose it’ stomatal regulation strategy with  
504 respect to soil moisture (Sperry *et al.*, 2017). SOX assumes plants with a more conservative water  
505 use strategy will be outcompeted by neighbouring plants with a less conservative stomatal  
506 behaviour (Wolf *et al.* 2016). The demographic consequences of the stomatal regulation strategy  
507 embedded in SOX should be explored in future studies using the dynamic vegetation component  
508 of JULES (Cox, 2001; Moore *et al.*, 2018). The more competitive soil moisture dynamics predicted  
509 by SOX, together with a more accurate representation of vegetation drought-induced mortality,  
510 which also can be developed from SOX, might be the key to predict sudden and widespread  
511 vegetation die-off during droughts that have been increasingly reported in ecosystems around the  
512 globe (Allen *et al.*, 2010; Worrall *et al.*, 2010; Meir *et al.*, 2015).

### 513 **Acknowledgments**

514 This research was supported by the Newton Fund through the Met Office Climate Science for  
515 Service Partnership Brazil (CSSP Brazil) and a NERC independent fellowship grant  
516 NE/N014022/1 to LR. This work used eddy covariance data acquired and shared by the FLUXNET  
517 community, including these networks: AmeriFlux, AfriFlux, AsiaFlux, CarboAfrica,  
518 CarboEuropeIP, CarboItaly, CarboMont, ChinaFlux, Fluxnet-Canada, GreenGrass, ICOS,  
519 KoFlux, LBA, NECC, OzFlux-TERN, TCOS-Siberia, and USCCC. The ERA-Interim reanalysis

520 data are provided by ECMWF and processed by LSCE. The FLUXNET eddy covariance data  
 521 processing and harmonization was carried out by the European Fluxes Database Cluster,  
 522 AmeriFlux Management Project, and Fluxdata project of FLUXNET, with the support of CDIAC  
 523 and ICOS Ecosystem Thematic Center, and the OzFlux, ChinaFlux and AsiaFlux offices.

#### 524 **Author contribution**

525 CBE, LR, MM, SS and PMC led the scientific development of SOX. PMC and CBE derived the  
 526 analytical solution. CBE evaluated leaf-level SOX using data provided by LR, PM, MM, TR, BM,  
 527 YW, TK, GST, RSO, ISM, BHPR. CBE and KW coded SOX into JULES. KW and AH created a  
 528 JULES suite used by CBE to evaluate JULES-SOX against eddy covariance data collected by KF,  
 529 GW, LM, among other FLUXNET and LBA PIs. All authors contributed to writing the manuscript.

#### 530 **References**

- 531 **Adams HD, Zeppel MJB, Anderegg WRL, Hartmann H, Landhäusser SM, Tissue DT,**  
 532 **Huxman TE, Hudson PJ, Franz TE, Allen CD, et al. 2017.** A multi-species synthesis of  
 533 physiological mechanisms in drought-induced tree mortality. *Nature Ecology and Evolution* **1**:  
 534 1285–1291.
- 535 **Alden CB, Miller JB, Gatti L V., Gloor MM, Guan K, Michalak AM, van der Laan-Luijkx**  
 536 **IT, Touma D, Andrews A, Basso LS, et al. 2016.** Regional atmospheric CO<sub>2</sub> inversion reveals  
 537 seasonal and geographic differences in Amazon net biome exchange. *Global change biology* **22**:  
 538 3427–3443.
- 539 **Allen CD, Macalady AK, Chenchouni H, Bachelet D, McDowell N, Vennetier M,**  
 540 **Kitzberger T, Rigling A, Breshears DD, Hogg EH (Ted., et al. 2010.** A global overview of  
 541 drought and heat-induced tree mortality reveals emerging climate change risks for forests. *Forest*  
 542 *Ecology and Management* **259**: 660–684.
- 543 **Anderegg WRL, Klein T, Bartlett M, Sack L, Pellegrini AFA, Choat B, Jansen S. 2016.**  
 544 Meta-analysis reveals that hydraulic traits explain cross-species patterns of drought-induced tree  
 545 mortality across the globe. *Proceedings of the National Academy of Sciences* **113**: 5024–5029.
- 546 **Anderegg WRL, Konings AG, Trugman AT, Yu K, Bowling DR, Gabbitas R, Karp DS,**  
 547 **Pacala S, Sperry JS, Sulman BN, et al. 2018a.** Hydraulic diversity of forests regulates

- 548 ecosystem resilience during drought. *Nature* **561**: 538.
- 549 **Anderegg WRL, Trugman AT, Bowling DR, Salvucci G, Tuttle SE. 2019.** Plant functional  
550 traits and climate influence drought intensification and land–atmosphere feedbacks. *Proceedings*  
551 *of the National Academy of Sciences of the United States of America* **116**: 14071–14076.
- 552 **Anderegg WRL, Wolf A, Arango-Velez A, Choat B, Chmura DJ, Jansen S, Kolb T, Li S,**  
553 **Meinzer FC, Pita P, et al. 2018b.** Woody plants optimise stomatal behaviour relative to  
554 hydraulic risk. *Ecology Letters* **21**: 968-977.
- 555 **Baldocchi D, Falge E, Gu L, Olson R, Hollinger D, Running S, Anthoni P, Bernhofer C,**  
556 **Davis K, Evans R, et al. 2001.** FLUXNET: A New Tool to Study the Temporal and Spatial  
557 Variability of Ecosystem-Scale Carbon Dioxide, Water Vapor, and Energy Flux Densities.  
558 *Bulletin of the American Meteorological Society* **82**: 2415–2434.
- 559 **Bartlett MK, Klein T, Jansen S, Choat B, Sack L. 2016.** The correlations and sequence of  
560 plant stomatal, hydraulic, and wilting responses to drought. *Proceedings of the National*  
561 *Academy of Sciences* **113**: 13098–13103.
- 562 **Berninger F, Hari P. 1993.** Optimal regulation of gas exchange: Evidence from field data.  
563 *Annals of Botany* **71**: 135–140.
- 564 **Best MJ, Pryor M, Clark DB, Rooney GG, Essery R, Ménard CB, Edwards JM, Hendry**  
565 **MA, Porson A, Gedney N. 2011.** The Joint UK Land Environment Simulator (JULES), model  
566 description–Part 1: energy and water fluxes. *Geoscientific Model Development* **4**: 677–699.
- 567 **Bonan GB, Williams M, Fisher RA, Oleson KW. 2014.** Modeling stomatal conductance in the  
568 earth system: Linking leaf water-use efficiency and water transport along the soil-plant-  
569 atmosphere continuum. *Geoscientific Model Development* **7**: 2193–2222.
- 570 **Bozdogan H. 1987.** Model selection and Akaike’s Information Criterion (AIC): The general  
571 theory and its analytical extensions. *Psychometrika* **52**: 345–370.
- 572 **Brodribb TJ, Holbrook NM, Edwards EJ, Gutiérrez M V. 2003.** Relations between stomatal  
573 closure, leaf turgor and xylem vulnerability in eight tropical dry forest trees. *Plant, Cell and*  
574 *Environment* **26**: 443–450.
- 575 **Buckley TN. 2017.** Modeling Stomatal Conductance. *Plant Physiology* **174**: 572–582.
- 576 **Buckley TN. 2019.** How do stomata respond to water status? *New Phytologist* **224**: 21-36.
- 577 **Carswell FE, Costa AL, Palheta M, Malhi Y, Meir P, Costa JDPR, Ruivo MDL, Leal**  
578 **LDSM, Costa JMN, Clement RJ, et al. 2002.** Seasonality in CO<sub>2</sub> and H<sub>2</sub>O flux at an eastern

- 579 Amazonian rain forest. *Journal of Geophysical Research D: Atmospheres* **107**: LBA-43.
- 580 **Choat B, Brodribb TJ, Brodersen CR, Duursma RA, López R, Medlyn BE. 2018.** Triggers  
581 of tree mortality under drought. *Nature* **558**: 531–539.
- 582 **Choat B, Jansen S, Brodribb TJ, Cochard H, Delzon S, Bhaskar R, Bucci SJ, Feild TS,**  
583 **Gleason SM, Hacked UG, et al. 2012.** Global convergence in the vulnerability of forests to  
584 drought. *Nature* **491**: 752–755.
- 585 **Clark DB, Mercado LM, Sitch S, Jones CD, Gedney N, Best MJ, Pryor M, Rooney GG,**  
586 **Essery RLH, Blyth E, et al. 2011.** The Joint UK Land Environment Simulator (JULES), Model  
587 description – Part 2: Carbon fluxes and vegetation. *Geoscientific Model Development*  
588 *Discussions* **4**: 641–688.
- 589 **Cosby BJ, Hornberger GM, Clapp RB, Ginn TR. 1984.** A Statistical Exploration of the  
590 Relationships of Soil Moisture Characteristics to the Physical Properties of Soils. *Water*  
591 *Resources Research* **20**: 682–690.
- 592 **da Costa ACL, Galbraith D, Almeida S, Portela BTT, da Costa M, de Athaydes Silva**  
593 **Junior J, Braga AP, de Gonçalves PHL, de Oliveira AA, Fisher R, et al. 2010.** Effect of 7 yr  
594 of experimental drought on vegetation dynamics and biomass storage of an eastern Amazonian  
595 rainforest. *New Phytologist* **187**: 579–591.
- 596 **da Costa ACL, Rowland L, Oliveira RS, Oliveira AAR, Binks OJ, Salmon Y, Vasconcelos**  
597 **SS, Junior JAS, Ferreira L V., Poyatos R, et al. 2018.** Stand dynamics modulate water cycling  
598 and mortality risk in droughted tropical forest. *Global Change Biology* **24**: 249–258.
- 599 **Cowan IR. 1986.** Economics of carbon fixation in higher plants. In: On the economy of plant  
600 form and function: proceedings of the Sixth Maria Moors Cabot Symposium, Evolutionary  
601 Constraints on Primary Productivity, Adaptive Patterns of Energy Capture in Plants, Harvard  
602 Forest, August 1983. Cambridge [Cambridgeshire]: Cambridge University Press, c1986.
- 603 **Cowan I. 2002.** Fit, fitter, fittest; where does optimisation fit in? *Silva Fennica* **36**: 745–754.
- 604 **Cowan IR, Farquhar GD. 1977.** Stomatal function in relation to leaf metabolism and  
605 environment. *Symposia of the Society for Experimental Biology* **31**: 471–505.
- 606 **Cox PM. 2001.** Description of the " TRIFFID " Dynamic Global Vegetation Model. *Hadley*  
607 *Centre technical note*.
- 608 **Cox PM, Betts RA, Jones CD, Spall SA, Totterdell IJ. 2000.** Acceleration of global warming  
609 due to carbon-cycle feedbacks in a coupled climate model. *Nature* **408**: 184.

- 610 **Cox PM, Huntingford C, Harding RJ. 1998.** A canopy conductance and photosynthesis model  
 611 for use in a GCM land surface scheme. *Journal of Hydrology* **212–213**: 79–94.
- 612 **Cramer MD, Hawkins HJ, Verboom GA. 2009.** The importance of nutritional regulation of  
 613 plant water flux. *Oecologia* **161**:15-24.
- 614 **Dewar RC, Franklin O, Mäkelä A, McMurtrie RE, Valentine HT. 2009.** Optimal Function  
 615 Explains Forest Responses to Global Change. *BioScience* **59**: 127-139.
- 616 **Dewar R, Mauranen A, Mäkelä A, Hölttä T, Medlyn B, Vesala T. 2018.** New insights into  
 617 the covariation of stomatal, mesophyll and hydraulic conductances from optimization models  
 618 incorporating nonstomatal limitations to photosynthesis. *New Phytologist* **217**: 571–585.
- 619 **Dharssi I, Vidale PL, Verhoef A, Macpherson B, Jones C, Best M. 2009.** New soil physical  
 620 properties implemented in the Unified Model at PS18. *Met Office technical report* **528**.
- 621 **Duffy PB, Brando P, Asner GP, Field CB. 2015.** Projections of future meteorological drought  
 622 and wet periods in the Amazon. *Proceedings of the National Academy of Sciences* **112**: 13172–  
 623 13177.
- 624 **Eller CB, Bittencourt PRL, Oliveira RS. 2018a.** Using sap flow to measure whole-tree  
 625 hydraulic conductance loss in response to drought. *Acta Horticulturae* **1222**: 75–84.
- 626 **Eller CB, Rowland L, Oliveira RS, Bittencourt PRL, Barros F V., da Costa ACL, Meir P,**  
 627 **Friend AD, Mencuccini M, Sitch S, et al. 2018b.** Modelling tropical forest responses to  
 628 drought and El Niño with a stomatal optimization model based on xylem hydraulics.  
 629 *Philosophical transactions of the Royal Society of London. Series B, Biological sciences* **373**:  
 630 20170315.
- 631 **Farquhar G, Schulze E, Kupperts M. 1980.** Responses to Humidity by Stomata of *Nicotiana*  
 632 *glauca* L. And *Corylus avellana* L. Are Consistent With the Optimization of Carbon Dioxide  
 633 Uptake With Respect to Water Loss. *Australian Journal of Plant Physiology* **7**: 315–327.
- 634 **Fisher RA, Williams M, Do Vale RL, Da Costa AL, Meir P. 2006.** Evidence from Amazonian  
 635 forests is consistent with isohydric control of leaf water potential. *Plant, Cell and Environment*  
 636 **20**: 151–165.
- 637 **Friend AD. 1995.** PGEN : an integrated model of leaf photosynthesis , and conductance.  
 638 *Ecological Modelling* **77**: 233–255.
- 639 **Friend AD, Cox PM. 1995.** Modelling the effects of atmospheric CO<sub>2</sub> on vegetation-atmosphere  
 640 interactions. *Agricultural and Forest Meteorology* **73**: 295.

- 641 **Goldstein G, Andrade JL, Meinzer FC, Holbrook NM, Cavelier J, Jackson P, Celis A. 1998.**  
642 Stem water storage and diurnal patterns of water use in tropical forest canopy trees. *Plant, Cell*  
643 *and Environment* **21**: 397-406.
- 644 **Goulden ML, Miller SD, Da Rocha HR, Menton MC, De Freitas HC, E Silva Figueira AM,**  
645 **Dias De Sousa CA. 2004.** Diel and seasonal patterns of tropical forest CO<sub>2</sub> exchange.  
646 *Ecological Applications* **14**: 42–54.
- 647 **Grace J, Lloyd J, McIntyre J, Miranda AC, Meir P, Miranda HS, Nobre C, Moncrieff J,**  
648 **Massheder J, Malhi Y, et al. 1995.** Carbon dioxide uptake by an undisturbed tropical rain forest  
649 in Southwest Amazonia, 1992 to 1993. *Science* **270**: 778–780.
- 650 **Harper AB, Cox PM, Friedlingstein P, Wiltshire AJ, Jones CD, Sitch S, Mercado LM,**  
651 **Groenendijk M, Robertson E, Kattge J, et al. 2016.** Improved representation of plant  
652 functional types and physiology in the Joint UK Land Environment Simulator (JULES v4.2)  
653 using plant trait information. *Geoscientific Model Development* **9**: 2415–2440.
- 654 **Hartmann H, Moura CF, Anderegg WRL, Ruehr NK, Salmon Y, Allen CD, Arndt SK,**  
655 **Breshears DD, Davi H, Galbraith D, et al. 2018.** Research frontiers for improving our  
656 understanding of drought-induced tree and forest mortality. *New Phytologist* **218**: 15–28.
- 657 **Hickler T, Prentice IC, Smith B, Sykes MT, Zaehle S. 2006.** Implementing plant hydraulic  
658 architecture within the LPJ Dynamic Global Vegetation Model. *Global Ecology and*  
659 *Biogeography* **15**: 567–577.
- 660 **Hubbard RM, Ryan MG, Stiller V, Sperry JS. 2001.** Stomatal conductance and  
661 photosynthesis vary linearly with plant hydraulic conductance in ponderosa pine. *Plant, Cell and*  
662 *Environment* **24**: 113–121.
- 663 **Jacobs C. 1994.** Direct impact of atmospheric CO<sub>2</sub> enrichment on regional transpiration.
- 664 **Kattge J, Díaz S, Lavorel S, Prentice IC, Leadley P, Bönisch G, Garnier E, Westoby M,**  
665 **Reich PB, Wright IJ, et al. 2011.** TRY - a global database of plant traits. *Global Change*  
666 *Biology* **17**: 2905–2935.
- 667 **Kennedy D, Swenson S, Oleson KW, Lawrence DM, Fisher R, Costa ACL da, Gentine P.**  
668 **2019.** Implementing plant hydraulics in the Community Land Model, version 5. *Journal of*  
669 *Advances in Modeling Earth Systems* **11**: 485-513.
- 670 **Klein T. 2014.** The variability of stomatal sensitivity to leaf water potential across tree species  
671 indicates a continuum between isohydric and anisohydric behaviours. *Functional Ecology* **28**:

- 672 1313–1320.
- 673 **Lens F, Picon-Cochard C, Delmas CEL, Signarbieux C, Buttler A, Cochard H, Jansen S,**  
 674 **Chauvin T, Doria LC, Del Arco M, et al. 2016.** Herbaceous angiosperms are not more  
 675 vulnerable to drought-induced embolism than angiosperm trees. *Plant Physiology* **172**: 661–667.
- 676 **Leuning R. 1995.** A critical appraisal of a combined stomatal - photosynthesis model for C3  
 677 plants. *Plant, Cell & Environment* **18**: 339–355.
- 678 **Lin Y, Medlyn B, Duursma R. 2015.** Optimal stomatal behaviour around the world. *Nature*  
 679 *Climate Change* **5**: 459.
- 680 **Loveland TR, Reed BC, Ohlen DO, Brown JF, Zhu Z, Yang L, Merchant JW. 2000.**  
 681 Development of a global land cover characteristics database and IGBP DISCover from 1 km  
 682 AVHRR data. *International Journal of Remote Sensing* **21**: 1303–1330.
- 683 **Mäkelä A, Berninger F, Hari P. 1996.** Optimal control of gas exchange during drought:  
 684 Theoretical analysis. *Annals of Botany* **77**: 461-468.
- 685 **Melotto M, Underwood W, He SY. 2008.** Role of stomata in plant innate immunity and foliar  
 686 bacterial diseases. *Annual Review of Phytopathology* **46**: 101-122.
- 687 **Manzoni S, Vico G, Palmroth S, Porporato A, Katul G. 2013.** Optimization of stomatal  
 688 conductance for maximum carbon gain under dynamic soil moisture. *Advances in Water*  
 689 *Resources* **62**: 90–105.
- 690 **Marengo JA, Souza CM, Thonicke K, Burton C, Halladay K, Betts RA, Alves LM, Soares**  
 691 **WR. 2018.** Changes in Climate and Land Use Over the Amazon Region: Current and Future  
 692 Variability and Trends. *Frontiers in Earth Science* **6**: 228.
- 693 **Martinez-Vilalta J, Poyatos R, Aguade D, Retana J, Mencuccini M. 2014.** A new look at  
 694 water transport regulation in plants. *New Phytologist* **204**: 105–115.
- 695 **Medlyn BE, Barton CVM, Broadmeadow MSJ, Ceulemans R, De Angelis P, Forstreuter M,**  
 696 **Freeman M, Jackson SB, Kellomäki S, Laitat E, et al. 2001.** Stomatal conductance of forest  
 697 species after long-term exposure to elevated CO2 concentration: A synthesis. *New Phytologist*  
 698 **149**: 247–264.
- 699 **Medlyn BE, Duursma RA, Eamus D, Ellsworth DS, Prentice IC, Barton CVM, Crous KY,**  
 700 **De Angelis P, Freeman M, Wingate L. 2011.** Reconciling the optimal and empirical  
 701 approaches to modelling stomatal conductance. *Global Change Biology* **17**: 2134–2144.
- 702 **Medlyn BE, De Kauwe MG, Zaehle S, Walker AP, Duursma RA, Luus K, Mishurov M,**



- 703 **Pak B, Smith B, Wang YP, et al. 2016.** Using models to guide field experiments: a priori  
704 predictions for the CO<sub>2</sub> response of a nutrient- and water-limited native Eucalypt woodland.  
705 *Global change biology* **22**: 2834–2851.
- 706 **Medlyn BE, Zaehle S, De Kauwe MG, Walker AP, Dietze MC, Hanson PJ, Hickler T, Jain**  
707 **AK, Luo Y, Parton W, et al. 2015.** Using ecosystem experiments to improve vegetation models.  
708 *Nature Climate Change* **5**: 528.
- 709 **Meinzer FC, Johnson DM, Lachenbruch B, McCulloh K a, Woodruff DR. 2009.** Xylem  
710 hydraulic safety margins in woody plants: Coordination of stomatal control of xylem tension  
711 with hydraulic capacitance. *Functional Ecology* **23**: 922–930.
- 712 **Meir P, Brando PM, Nepstad D, Vasconcelos S, Costa ACL, Davidson E, Almeida S, Fisher**  
713 **RA, Sotta ED, Zarin D, et al. 2009.** *Amazonia and Global Change* (J Gash, M Keller, M  
714 Bustamante, and P Silva Dias, Eds.). American Geophysical Union.
- 715 **Meir P, Wood TE, Galbraith DR, Brando PM, Da Costa ACL, Rowland L, Ferreira L V.**  
716 **2015.** Threshold Responses to Soil Moisture Deficit by Trees and Soil in Tropical Rain Forests:  
717 Insights from Field Experiments. *BioScience* **65**: 882–892.
- 718 **Meir P, Mencuccini M, Binks O, da Costa AL, Ferreira L, et al. 2018.** Short-term effects of  
719 drought on tropical forest do not fully predict impacts of repeated or long-term drought: gas  
720 exchange versus growth. *Philosophical Transactions of the Royal Society B: Biological Sciences*,  
721 **373**(1760): 20170311.
- 722 **Mencuccini M, Manzoni S, Christoffersen B. 2019a.** Modelling water fluxes in plants: from  
723 tissues to biosphere. *New Phytologist* **222**: 1207–1222.
- 724 **Mencuccini M, Rosas T, Rowland L, Choat B, Cornelissen JHC, Jansen S, Kramer K,**  
725 **Lepenas A, Manzoni S, Niinemets U, Reich P, Schrod F, Soudzilovskaia NA, Wright I,**  
726 **Martinez-Vilalta J, 2019b.** Leaf economics and xylem hydraulics drive leaf/wood area ratios.  
727 *New Phytologist* doi.org/10.1111/nph.15998.
- 728 **Mercado LM, Bellouin N, Sitch S, Boucher O, Huntingford C, Wild M, Cox PM. 2009.**  
729 Impact of changes in diffuse radiation on the global land carbon sink. *Nature* **458**: 1014.
- 730 **Mercado LM, Huntingford C, Gash JHC, Cox PM, Jogireddy V. 2007.** Improving the  
731 representation of radiation interception and photosynthesis for climate model applications.  
732 *Tellus, Series B: Chemical and Physical Meteorology* **59**: 553–565.
- 733 **Moore JR, Zhu K, Huntingford C, Cox PM. 2018.** Equilibrium forest demography explains

- 734 the distribution of tree sizes across North America. *Environmental Research Letters* **13**: 084019.
- 735 **Mott KA. 1988.** Do Stomata Respond to CO<sub>2</sub> Concentrations Other than Intercellular? *Plant*  
736 *Physiology* **86**: 200–203.
- 737 **Nash JE, Sutcliffe JV. 1970.** River flow forecasting through conceptual models part I — A  
738 discussion of principles. *Journal of Hydrology* **10**: 282–290.
- 739 **Nepstad DC, De Carvalho CR, Davidson EA, Jipp PH, Lefebvre PA, Negreiros GH, Da**  
740 **Silva ED, Stone TA, Trumbore SE, Vieira S. 1994.** The role of deep roots in the hydrological  
741 and carbon cycles of Amazonian forests and pastures. *Nature* **372**: 666–669.
- 742 **Ocheltree TW, Nippert JB, Prasad PVV. 2016.** A safety vs efficiency trade-off identified in  
743 the hydraulic pathway of grass leaves is decoupled from photosynthesis, stomatal conductance  
744 and precipitation. *New Phytologist* **210**: 97–107.
- 745 **Oliveira RS, Costa FRC, van Baalen E, de Jonge A, Bittencourt PR, Almanza Y, Barros F**  
746 **de V., Cordoba EC, Fagundes M V., Garcia S, et al. 2019.** Embolism resistance drives the  
747 distribution of Amazonian rainforest tree species along hydro-topographic gradients. *New*  
748 *Phytologist* **221**: 1457–1465.
- 749 **Powell TL, Galbraith DR, Christoffersen BO, Harper A, Imbuzeiro HMA, Rowland L,**  
750 **Almeida S, Brando PM, da Costa ACL, Costa MH, et al. 2013.** Confronting model  
751 predictions of carbon fluxes with measurements of Amazon forests subjected to experimental  
752 drought. *New Phytologist* **200**: 350–365.
- 753 **Prentice IC, Dong N, Gleason SM, Maire V, Wright IJ. 2014.** Balancing the costs of carbon  
754 gain and water transport: testing a new theoretical framework for plant functional ecology.  
755 *Ecology letters* **17**: 82-91.
- 756 **Qu X, Cao B, Kang J, Wang X, Han X, Jiang W, et al. 2019.** Fine-tuning stomatal movement  
757 through small signaling peptides. *Frontiers in plant science* **10**: 69.
- 758 **Restrepo-Coupe N, Levine NM, Christoffersen BO, Albert LP, Wu J, Costa MH, Galbraith**  
759 **D, Imbuzeiro H, Martins G, da Araujo AC, et al. 2017.** Do dynamic global vegetation models  
760 capture the seasonality of carbon fluxes in the Amazon basin? A data-model intercomparison.  
761 *Global Change Biology* **23**: 191–208.
- 762 **Rogers A, Medlyn BE, Dukes JS, Bonan G, von Caemmerer S, Dietze MC, Kattge J,**  
763 **Leakey ADB, Mercado LM, Niinemets U, et al. 2017.** A roadmap for improving the  
764 representation of photosynthesis in Earth system models. *New Phytologist* **213**: 22–42.

- 765 **Rowland L, Da Costa ACL, Galbraith DR, Oliveira RS, Binks OJ, Oliveira AAR, Pullen**  
766 **AM, Doughty CE, Metcalfe DB, Vasconcelos SS, et al. 2015.** Death from drought in tropical  
767 forests is triggered by hydraulics not carbon starvation. *Nature* **528**: 119–122.
- 768 **Saleska SR, da Rocha HR, Huete AR, Nobre AD, Artaxo P, Shimabukuro YE. 2013.** LBA-  
769 ECO CD-32 Flux Tower Network Data Compilation, Brazilian Amazon: 1999-2006. Data set.  
770 *Oak Ridge National Laboratory Distributed Active Archive Center, Oak Ridge, Tennessee, USA.*
- 771 **Savage VM, Bentley LP, Enquist BJ, Sperry JS, Smith DD, Reich PB, von Allmen EI. 2010.**  
772 Hydraulic trade-offs and space filling enable better predictions of vascular structure and function  
773 in plants. *Proceedings of the National Academy of Sciences of the United States of America* **107**:  
774 22722–22727.
- 775 **Sellers PJ. 1985.** Canopy reflectance, photosynthesis and transpiration. *International Journal of*  
776 *Remote Sensing* **6**: 1335–1372.
- 777 **Sheffield J, Wood EF. 2008.** Projected changes in drought occurrence under future global  
778 warming from multi-model, multi-scenario, IPCC AR4 simulations. *Climate Dynamics* **31**: 79–  
779 105.
- 780 **Sitch S, Huntingford C, Gedney N, Levy PE, Lomas M, Piao SL, Betts R, Ciais P, Cox P,**  
781 **Friedlingstein P, et al. 2008.** Evaluation of the terrestrial carbon cycle, future plant geography  
782 and climate-carbon cycle feedbacks using five Dynamic Global Vegetation Models (DGVMs).  
783 *Global Change Biology* **14**: 2015–2039.
- 784 **Sperry JS. 2004.** Coordinating stomatal and xylem functioning—an evolutionary perspective.  
785 *New Phytologist* **162**: 568-570.
- 786 **Sperry JS, Venturas MD, Anderegg WRL, Mencuccini M, Mackay DS, Wang Y, Love DM.**  
787 **2017.** Predicting stomatal responses to the environment from the optimization of photosynthetic  
788 gain and hydraulic cost. *Plant Cell and Environment* **40**: 816–830.
- 789 **Stocker BD, Zscheischler J, Keenan TF, Prentice IC, Peñuelas J, Seneviratne SI. 2018.**  
790 Quantifying soil moisture impacts on light use efficiency across biomes. *New Phytologist* **218**:  
791 1430–1449.
- 792 **Ukkola AM, De Kauwe MG, Pitman AJ, Best MJ, Abramowitz G, Haverd V, Decker M,**  
793 **Haughton N. 2016.** Land surface models systematically overestimate the intensity, duration and  
794 magnitude of seasonal-scale evaporative droughts. *Environmental Research Letters* **11**: 104012.
- 795 **Venturas MD, Sperry JS, Love DM, Frehner EH, Allred MG, Wang Y, Anderegg WRL.**

- 796       **2018.** A stomatal control model based on optimization of carbon gain versus hydraulic risk  
797               predicts aspen sapling responses to drought. *New Phytologist* **220**: 835–850.
- 798       **Walsh RPD, Lawler DM. 1981.** Rainfall Seasonality: Description, Spatial Patterns and Change  
799               Through Time. *Weather* **36**: 201–208.
- 800       **Wang Y, Sperry JS, Venturas MD, Trugman AT, Love DM, Anderegg WR. 2019.** The  
801       stomatal response to rising CO<sub>2</sub> concentration and drought is predicted by a hydraulic trait-based  
802               optimization model. *Tree Physiology*.
- 803       **Williams M, Rastetter EB, Fernandes DN, Goulden ML, Wofsy SC, Shaver GR, Melillo**  
804       **JM, Munger JW, Fan SM, Nadelhoffer KJ. 1996.** Modelling the soil-plant-atmosphere  
805       continuum in a Quercus-acer stand at Harvard forest: The regulation of stomatal conductance by  
806       light, nitrogen and soil/plant hydraulic properties. *Plant, Cell and Environment* **19**: 911–927.
- 807       **Winkler AJ, Myneni RB, Alexandrov GA, Brovkin V. 2019.** Earth system models  
808       underestimate carbon fixation by plants in the high latitudes. *Nature Communications* **10**.
- 809       **Wolf A, Anderegg WRL, Pacala SW. 2016.** Optimal stomatal behavior with competition for  
810       water and risk of hydraulic impairment. *Proceedings of the National Academy of Sciences* **113**:  
811               E7222–E7230.
- 812       **Wolfe BT, Sperry JS, Kursar TA. 2016.** Does leaf shedding protect stems from cavitation  
813       during seasonal droughts? A test of the hydraulic fuse hypothesis. *New Phytologist* **212**: 1007–  
814               1018.
- 815       **Worrall JJ, Marchetti SB, Egeland L, Mask RA, Eager T, Howell B. 2010.** Effects and  
816       etiology of sudden aspen decline in southwestern Colorado, USA. *Forest Ecology and*  
817               *Management* **260**: 638–648.
- 818       **Xu X, Medvigy D, Powers JS, Becknell JM, Guan K. 2016.** Diversity in plant hydraulic traits  
819       explains seasonal and inter-annual variations of vegetation dynamics in seasonally dry tropical  
820               forests. *New Phytologist* **212**: 80-95.

821  
822  
823  
824  
825  
826

827  
828  
829  
830  
831  
832

833 **Figure captions.**

834 **Figure 1.** SOX stomatal conductance ( $g_s$ ) sensitivity to environmental drivers in **(a)** (vapour  
835 pressure deficit,  $D$ ; pre-dawn water potential,  $\Psi_{pd}$ , Incident photosynthetically active radiation,  $I_{par}$ ,  
836 and atmospheric CO<sub>2</sub> partial pressure,  $c_a$ ) and plant hydraulic traits in **(b)** ( $\Psi$  when plant loses 50%  
837 of its maximum conductance,  $\Psi_{50}$ ; shape of vulnerability function,  $a$ ; and minimum plant hydraulic  
838 resistance,  $r_{pmin}$ ). The variables were changed individually while the others were held constant at  
839 their reference values ( $D = 0.5$  kPa,  $\Psi_{pd} = -0.5$  MPa,  $I_{par} = 600$   $\mu\text{mol m}^{-2} \text{s}^{-1}$ ,  $c_a = 36$  Pa,  $\Psi_{50} = -2$   
840 MPa,  $a = 3$ ,  $r_{pmin} = 1$   $\text{m}^2 \text{s MPa mmol}^{-1}$ ). For the panels **(c)** and **(d)** the reference lines (dashed  
841 black) represents values of  $\Psi_{50} = -3$  MPa,  $a = 5$ ,  $r_{pmin} = 1$   $\text{mmol}^{-1} \text{m}^2 \text{s MPa}$ , the coloured lines show  
842 how changing each hydraulic parameter affects  $g_s$  response to  $\Psi_{pd}$  and  $D$ . The  $I_{par}$  was set to 2000  
843  $\mu\text{mol m}^{-2} \text{s}^{-1}$  in panels **(c)** and **(d)**. The  $V_{cmax25}$  was set to 100  $\mu\text{mol m}^{-2} \text{s}$  and the rest of the  
844 photosynthetic parameters follow the BET-Tr parameterization from Harper *et al.* (2016).

845 **Figure 2.** Predicted and observed (grey points) stomatal conductance ( $g_s$ ) response to changes in  
846 leaf pre-dawn water potential ( $\Psi_{pd}$ ) for the woody plant functional types (PFT) from Harper *et al.*  
847 (2016), except for Needleleaf deciduous trees which was not present in the dataset used in this  
848 study. The red lines are SOX and  $\beta$ -function (Eqn 7-8) best fit. The shaded regions are non-  
849 parametric 95% confidence boundaries derived from 1000 bootstrapping replications of the SOX  
850 hydraulic inputs. All environmental conditions except  $\Psi_{pd}$  were held constant at their median  
851 values when the  $g_s$  measurements were taken. The  $\Psi_{pd}$  was transformed in soil volumetric water

852 content to drive the  $\beta$ -function using Clapp & Hornberger (1978) equations parameterized with  
 853 soil physical properties derived from the Met Office Central Ancillary Program (Dharssi *et al.*,  
 854 2009). The model fit to data is shown as the root mean squared errors (RMSE) and Nash-Sutcliffe  
 855 (1970) model efficiency index (NSE). The PFT abbreviations are: BET-Tr (Broadleaf evergreen  
 856 tropical tree), BET-Te (Broadleaf evergreen temperate tree), BDT (Broadleaf deciduous tree),  
 857 NET (Needleleaf evergreen tree), ESh (Evergreen shrubs) and DSh (Deciduous shrubs).

858 **Figure 3.** Monthly mean gross primary production (GPP) modelled by default JULES (blue line)  
 859 and JULES-SOX (red line) versus observations (grey points are means and bars are 2xSE) at each  
 860 eddy flux site used for calibrating the SOX hydraulic parameters (PFT; Table S2 and Fig. S3). The  
 861 model fit to data is shown as the root mean squared errors (RMSE) and Nash-Sutcliffe (1970)  
 862 model efficiency index (NSE). The PFT abbreviations are: BET-Tr (Broadleaf evergreen tropical  
 863 tree), BET-Te (Broadleaf evergreen temperate tree), BDT (Broadleaf deciduous tree), NET  
 864 (Needleleaf evergreen tree), NDT (Needleleaf deciduous tree), C<sub>3</sub> (C<sub>3</sub> grasses), C<sub>4</sub> (C<sub>4</sub> grasses),  
 865 ESh (Evergreen shrubs) and DSh (Deciduous shrubs).

866 **Figure 4.** Minimum observed midday leaf water potential ( $\Psi_{midday}$ ) from 279 woody plant species  
 867 compiled from the literature grouped using the Harper *et al.* (2016) plant functional types (PFT)  
 868 categories. The SOX modelled  $\Psi_{midday}$  for each of the calibration sites (see Table S2 and Fig. S2)  
 869 is plotted in red. The circle is the mean  $\Psi_{midday}$  and the arrows indicate the minimum and maximum  
 870  $\Psi_{midday}$ . The data for the deciduous PFT was restricted to the growing season. The PFT  
 871 abbreviations are: BET-Tr (Broadleaf evergreen tropical tree), BET-Te (Broadleaf evergreen  
 872 temperate tree), BDT (Broadleaf deciduous tree), NET (Needleleaf evergreen tree), NDT  
 873 (Needleleaf deciduous tree), C<sub>3</sub> (C<sub>3</sub> grasses), C<sub>4</sub> (C<sub>4</sub> grasses), ESh (Evergreen shrubs) and DSh  
 874 (Deciduous shrubs).

875 **Figure 5.** The Taylor diagram (**a**) shows the difference in JULES and JULES-SOX skill to predict  
876 the monthly GPP in each biome. Green lines are the model centered root mean squared errors  
877 (RMSE), points closer to the reference circle in the x-axis indicate higher model skill. The two  
878 arrows highlight the improvement in model skill for EBF-Tr and EBF-Te. The boxplot panels  
879 show the differences between models (default JULES in blue and JULES-SOX in red) and  
880 observations in the annual gross primary productivity (GPP in **b**) and the GPP seasonality (GPP  
881 SI in **c**). Data gaps were excluded from the annual GPP calculations for both models and  
882 observations, therefore the differences can be used to evaluate the model skill, but the absolute  
883 values do not represent the total annual GPP in each biome. The GPP SI was computed using the  
884 approach from Walsh and Lawler (1981). Boxes filled with lines are different (at  $\alpha=0.05$ ) from 0  
885 in a one sample t-test. The biome abbreviations are: Cropland (CRO), deciduous broadleaf forests  
886 (DBF), deciduous needleleaf forests (DNF), temperate evergreen broadleaf forests (EBF-Te),  
887 tropical evergreen broadleaf forests (EBF-Tr), evergreen needleleaf forest (ENF), grassland  
888 (GRA), mixed forest (MF), savannah (SAV), shrubland (SHR), and wetlands (WET).

889 **Figure 6.** Model predictions of the normalised light-use efficiency responses to soil moisture,  
890 expressed as a fraction of the soil moisture saturation point at the top 1 m of soil. The light use  
891 efficiency is computed as the ratio between gross primary productivity and the photosynthetic  
892 active radiation absorbed by the canopy. The default JULES predictions are in blue and JULES-  
893 SOX predictions in red. The lines in the scatter plot panels are linear regressions fit to the data.  
894 The histograms on the bottom panels are the soil moisture probability density predicted by each  
895 model. The biome abbreviations are: Cropland (CRO), deciduous broadleaf forests (DBF),  
896 deciduous needleleaf forests (DNF), temperate evergreen broadleaf forests (EBF-Te), tropical

897 evergreen broadleaf forests (EBF-Tr), evergreen needleleaf forest (ENF), grassland (GRA), mixed  
 898 forest (MF), savannah (SAV), shrubland (SHR), and wetlands (WET).

899

900

901

902

903 **Tables.**

904 **Table 1.** Residual sum of squares (RSS), number of leaf-level stomatal conductance observations  
 905 (N) used to fit  $n$  parameters to the data, and the resulting Akaike Information Criterion differences  
 906 ( $\Delta$ AIC) between SOX and the  $\beta$ -function.

PFT	N	SOX		$\beta$ -function		$\Delta$ AIC
		RSS	$n$	RSS	$n$	
<i>BET-Tr</i>	434	4.83	3	6.53	2	-126.1
<i>BET-Te</i>	1334	19.68	3	37.37	2	-853.2
<i>BDT</i>	71	3.48	3	3.04	2	11.6
<i>NET</i>	1571	0.65	3	2.29	2	-1926.4
<i>ESh</i>	133	3.37	3	7.94	2	-112
<i>DSh</i>	64	2.76	3	8.03	2	-66.4

907

908 **Table 2.** Observed (*Obs*) mean ( $\pm$ SD) hydraulic parameters compiled from literature for each plant  
 909 functional type (PFT) from JULES (Harper *et al.* 2016). The calibrated (*Cal*) columns are the  
 910 parameter values that maximize JULES-SOX fit to observed GPP in the calibration sites (see Table  
 911 S2 and Fig. S2).

PFT	$\Psi_{50}$ (MPa)			$a$ (unitless)			$r_{pmin}$ (mmol <sup>-1</sup> m <sup>2</sup> s MPa)		
	N	<i>Obs</i>	<i>Cal</i>	N	<i>Obs</i>	<i>Cal</i>	N	<i>Obs</i>	<i>Cal</i>
<i>BET-Tr</i>	77	-1.9( $\pm$ 1.3)	-1.7	20	4.4( $\pm$ 2.1)	2.1	40	2.2( $\pm$ 3.4)	0.6
<i>BET-Te</i>	44	-2.7( $\pm$ 1.5)	-1.8	17	3.7( $\pm$ 1.8)	2.8	40	3.1( $\pm$ 8)	5



<i>BDT</i>	87	-2.6( $\pm$ 1.4)	-1.6	43	5.5( $\pm$ 3.8)	3.5	31	5.3( $\pm$ 5.6)	0.5
<i>NET</i>	48	-4.2( $\pm$ 1.2)	-2.6	25	8.7( $\pm$ 4.9)	4.9	20	2.4( $\pm$ 1.8)	4.2
<i>NDT</i>	5	-3.4( $\pm$ 0.6)	-1.8	2	7.4( $\pm$ 5)	1.8	2	8( $\pm$ 4.3)	9
<i>C<sub>3</sub></i>	45	-3.1( $\pm$ 1.6)	-2.4	-	-	2.2	-	-	3.2
<i>C<sub>4</sub></i>	15	-2.7( $\pm$ 1.7)	-1.5	-	-	1.8	-	-	9.5
<i>ESh</i>	61	-4( $\pm$ 2.2)	-2.1	53	4.1( $\pm$ 3.3)	2.5	49	1.5( $\pm$ 1.8)	9.5
<i>DSh</i>	26	-4( $\pm$ 2.3)	-1.8	3	3.4( $\pm$ 2.2)	2.1	4	2.6( $\pm$ 2.4)	5

912 *Note: The N column is the number of species compiled for the correspondent parameter.*

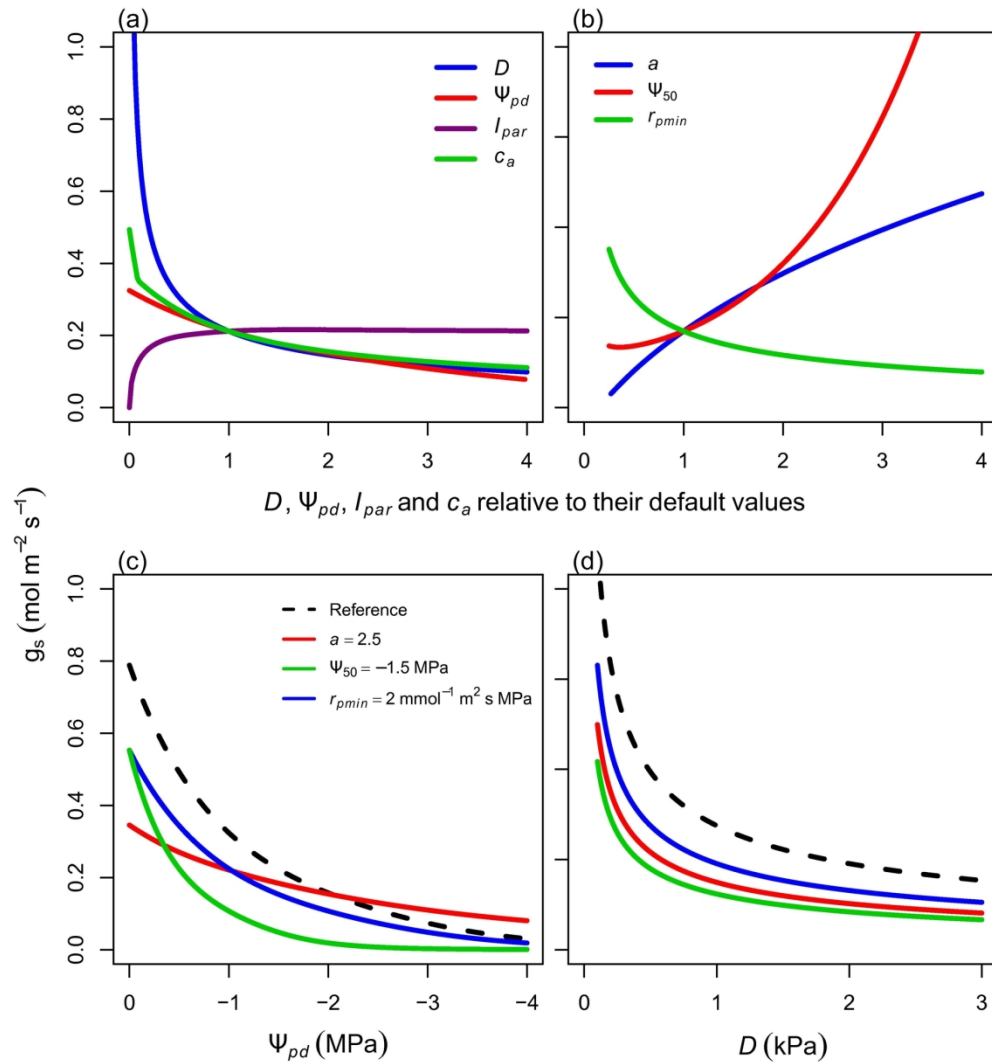
913

914 **Table 3.** Median Nash-Sutcliffe (1970) model efficiency index (NSE) and root mean square error

915 (RMSE) for the biomes used for evaluating JULES-SOX and default JULES.

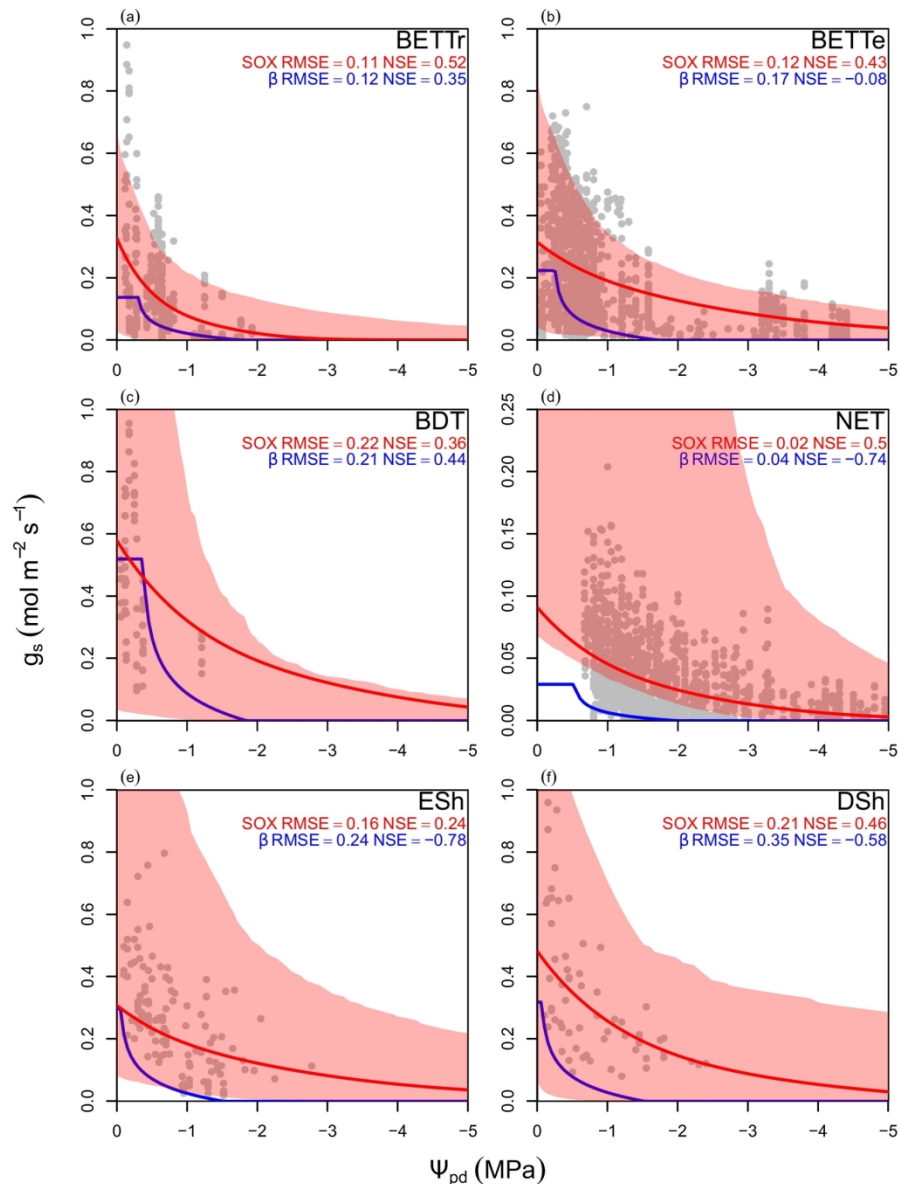
Biome	N	<i>JULES-SOX</i>		<i>JULES</i>	
		NSE	RMSE	NSE	RMSE
<i>CRO</i>	3	0.49	123.12	0.57	141.1
<i>DBF</i>	7	0.89	37.32	0.83	47.19
<i>DNF</i>	1	0.58	25.93	0.37	31.97
<i>EBF-Te</i>	3	-0.23	45.22	-1.24	66.36
<i>EBF-Tr</i>	6	0.41	40.36	-2.77	73.53
<i>ENF</i>	5	0.9	34.14	0.59	40.58
<i>GRA</i>	12	0.22	32.31	-0.01	30.62
<i>MF</i>	3	0.85	47.87	0.59	79.29
<i>SAV</i>	5	-0.4	59.72	-2.12	89.69
<i>SHR</i>	4	0.78	14.90	0.64	15.92
<i>WET</i>	21	0.68	32.23	0.46	38.67

916 *Note: The N column is the number of sites representing the biome in the eddy flux dataset*



SOX stomatal conductance ( $g_s$ ) sensitivity to environmental drivers in (a) (vapour pressure deficit,  $D$ ; pre-dawn water potential,  $\Psi_{pd}$ , Incident photosynthetically active radiation,  $I_{par}$ , and atmospheric CO<sub>2</sub> partial pressure,  $c_a$ ) and plant hydraulic traits in (b) ( $\Psi$  when plant loses 50% of its maximum conductance,  $\Psi_{50}$ ; shape of vulnerability function,  $a$ ; and minimum plant hydraulic resistance,  $r_{pmin}$ ). The variables were changed individually while the others were held constant at their reference values ( $D = 0.5$  kPa,  $\Psi_{pd} = -0.5$  MPa,  $I_{par} = 600$   $\mu\text{mol m}^{-2} \text{s}^{-1}$ ,  $c_a = 36$  Pa,  $\Psi_{50} = -2$  MPa,  $a = 3$ ,  $r_{pmin} = 1$  m<sup>2</sup> s MPa mmol<sup>-1</sup>). For the panels (c) and (d) the reference lines (dashed black) represents values of  $\Psi_{50} = -3$  MPa,  $a = 5$ ,  $r_{pmin} = 1$  mmol<sup>-1</sup> m<sup>2</sup> s MPa, the coloured lines show how changing each hydraulic parameter affects  $g_s$  response to  $\Psi_{pd}$  and  $D$ . The  $I_{par}$  was set to 2000  $\mu\text{mol m}^{-2} \text{s}^{-1}$  in panels (c) and (d). The  $V_{cmax25}$  was set to 100  $\mu\text{mol m}^{-2} \text{s}^{-1}$  and the rest of the photosynthetic parameters follow the BET-Tr parameterization from Harper et al. (2016).

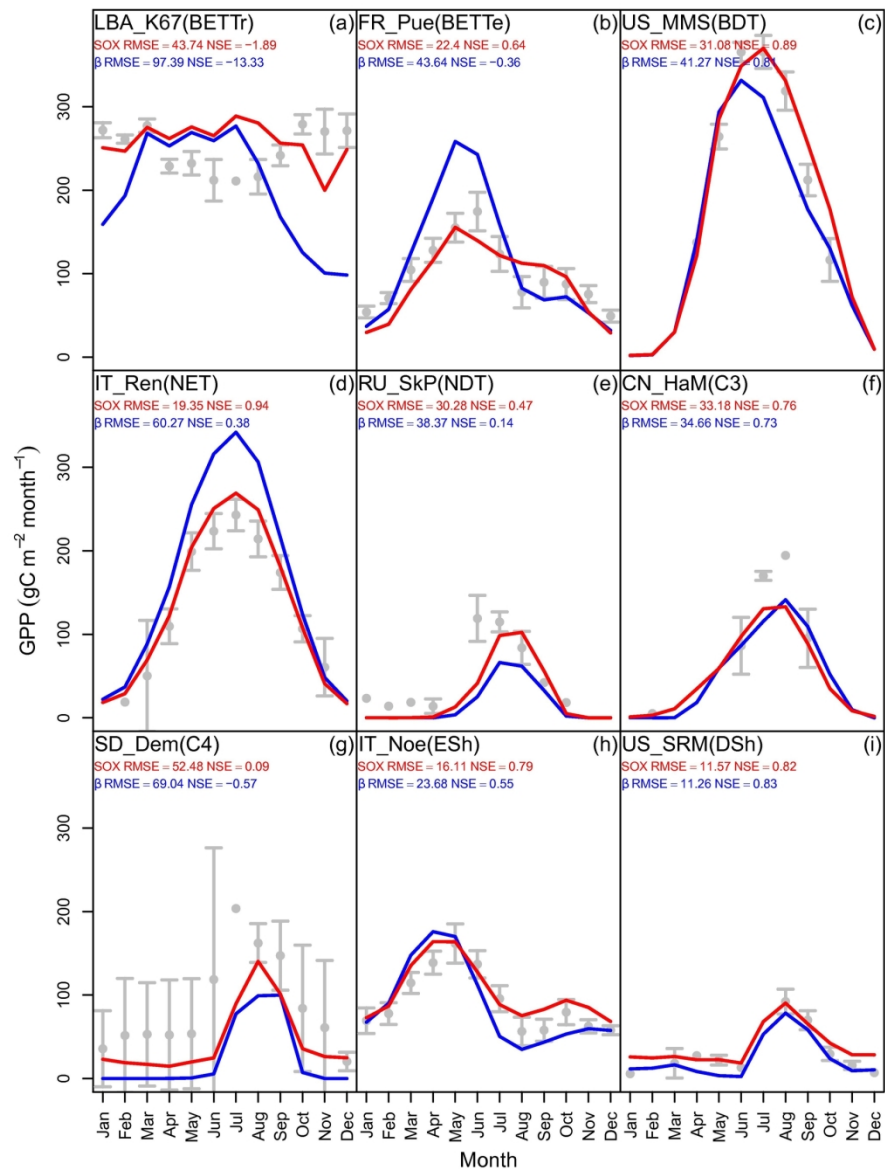
166x188mm (300 x 300 DPI)



Predicted and observed (grey points) stomatal conductance ( $g_s$ ) response to changes in leaf pre-dawn water potential ( $\Psi_{pd}$ ) for the woody plant functional types (PFT) from Harper et al. (2016), except for Needleleaf deciduous trees which was not present in the dataset used in this study. The red lines are SOX and  $\beta$ -function (Eqn 7-8) best fit. The shaded regions are non-parametric 95% confidence boundaries derived from 1000 bootstrapping replications of the SOX hydraulic inputs. All environmental conditions except  $\Psi_{pd}$  were held constant at their median values when the  $g_s$  measurements were taken. The  $\Psi_{pd}$  was transformed in soil volumetric water content to drive the  $\beta$ -function using Clapp & Hornberger (1978) equations parameterized with soil physical properties derived from the Met Office Central Ancillary Program (Dharssi et al., 2009). The model fit to data is shown as the root mean squared errors (RMSE) and Nash-Sutcliffe (1970) model efficiency index (NSE). The PFT abbreviations are: BET-Tr (Broadleaf evergreen tropical tree), BET-Te (Broadleaf evergreen temperate tree), BDT (Broadleaf deciduous tree), NET (Needleleaf evergreen tree), ESh (Evergreen shrubs) and DSh (Deciduous shrubs).

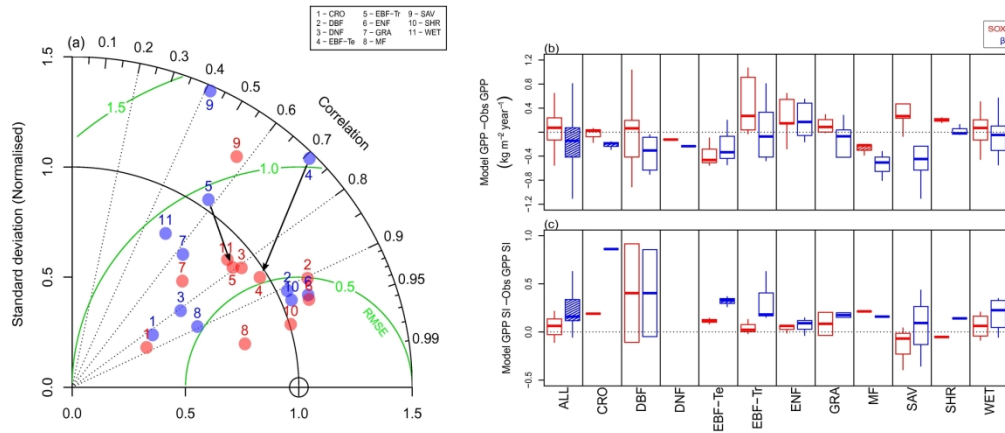
152x203mm (300 x 300 DPI)





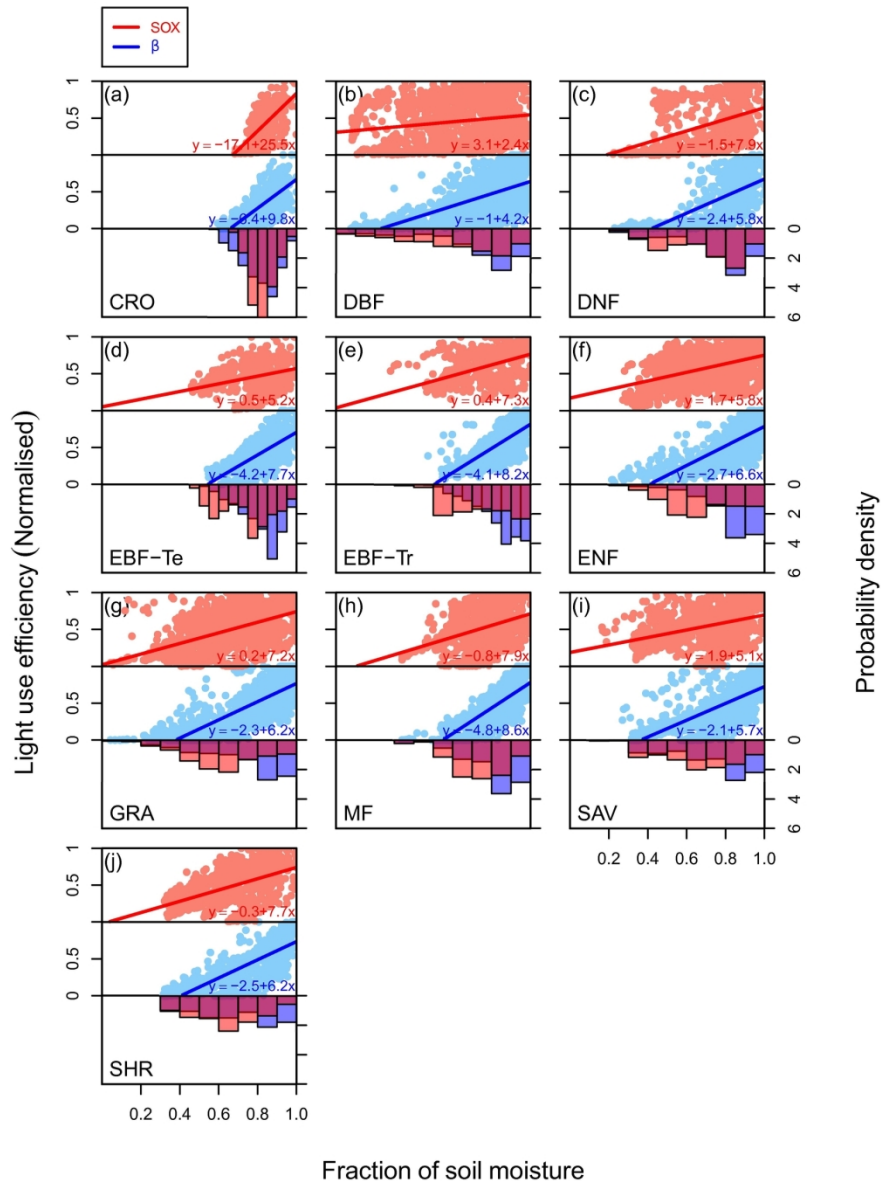
Monthly mean gross primary production (GPP) modelled by default JULES (blue line) and JULES-SOX (red line) versus observations (grey points are means and bars are  $2 \times \text{SE}$ ) at each eddy flux site used for calibrating the SOX hydraulic parameters (PFT; Table S2 and Fig. S3). The model fit to data is shown as the root mean squared errors (RMSE) and Nash-Sutcliffe (1970) model efficiency index (NSE). The PFT abbreviations are: BET-Tr (Broadleaf evergreen tropical tree), BET-Te (Broadleaf evergreen temperate tree), BDT (Broadleaf deciduous tree), NET (Needleleaf evergreen tree), NDT (Needleleaf deciduous tree), C3 (C3 grasses), C4 (C4 grasses), ESh (Evergreen shrubs) and DSh (Deciduous shrubs).

152x203mm (300 x 300 DPI)



The Taylor diagram (a) shows the difference in JULES and JULES-SOX skill to predict the monthly GPP in each biome. Green lines are the model centered root mean squared errors (RMSE), points closer to the reference circle in the x-axis indicate higher model skill. The two arrows highlight the improvement in model skill for EBF-Te and EBF-Tr. The boxplot panels show the differences between models (default JULES in blue and JULES-SOX in red) and observations in the annual gross primary productivity (GPP in b) and the GPP seasonality (GPP SI in c). Data gaps were excluded from the annual GPP calculations for both models and observations, therefore the differences can be used to evaluate the model skill, but the absolute values do not represent the total annual GPP in each biome. The GPP SI was computed using the approach from Walsh and Lawler (1981). Boxes filled with lines are different (at  $\alpha=0.05$ ) from 0 in a one sample t-test. The biome abbreviations are: Cropland (CRO), deciduous broadleaf forests (DBF), deciduous needleleaf forests (DNF), temperate evergreen broadleaf forests (EBF-Te), tropical evergreen broadleaf forests (EBF-Tr), evergreen needleleaf forest (ENF), grassland (GRA), mixed forest (MF), savannah (SAV), shrubland (SHR), and wetlands (WET).

218x93mm (300 x 300 DPI)



Model predictions of the normalised light-use efficiency responses to soil moisture, expressed as a fraction of the soil moisture saturation point at the top 1 m of soil. The light use efficiency is computed as the ratio between gross primary productivity and the photosynthetic active radiation absorbed by the canopy. The default JULES predictions are in blue and JULES-SOX predictions in red. The lines in the scatter plot panels are linear regressions fit to the data. The histograms on the bottom panels are the soil moisture probability density predicted by each model. The biome abbreviations are: Cropland (CRO), deciduous broadleaf forests (DBF), deciduous needleleaf forests (DNF), temperate evergreen broadleaf forests (EBF-Te), tropical evergreen broadleaf forests (EBF-Tr), evergreen needleleaf forest (ENF), grassland (GRA), mixed forest (MF), savannah (SAV), shrubland (SHR), and wetlands (WET).

152x203mm (300 x 300 DPI)